J. Fluid Mech. (2015), *vol.* 765, *pp.* 353–395. © Cambridge University Press 2015
doi:10.1017/jfm.2014.683

Drag reduction in heated channels

Daniel Floryan[1,‡] **and J. M. Floryan**[1,†]

[1]Department of Mechanical and Materials Engineering, The University of Western Ontario, London, Ontario, N6A 5B9, Canada

(Received 23 February 2014; revised 4 October 2014; accepted 20 November 2014; first published online 23 January 2015)

It is known that the drag for flows driven by a pressure gradient in heated channels can be reduced below the level found in isothermal channels. This reduction occurs for spatially modulated heating and is associated with the formation of separation bubbles which isolate the main stream from direct contact with the solid wall. It is demonstrated that the use of a proper combination of spatially distributed and spatially uniform heating components results in an increase in the horizontal and vertical temperature gradients which lead to an intensification of convection which, in turn, significantly increases the drag reduction. An excessive increase of the uniform heating leads to breakup of the bubbles and the formation of complex secondary states, resulting in a deterioration of the system performance. This performance may, under certain conditions, still be better than that achieved using only spatially distributed heating. Detailed calculations have been carried out for the Prandtl number $Pr = 0.71$ and demonstrate that this technique is effective for flows with a Reynolds number $Re < 10$; faster flows wash away separation bubbles. The question of net gain remains to be settled as it depends on the method used to achieve the desired wall temperature and on the cost of the required energy. The presented results provide a basis for the design of passive flow control techniques utilizing heating patterns as controlling agents.

Key words: drag reduction, flow control

1. Introduction

The principal motivation for the development of drag reducing techniques is the desire to reduce energy costs associated with transportation. The mechanisms responsible for drag generation can be conveniently categorized as those associated with the pressure form drag, the pressure interaction drag and the shear drag (Mohammadi & Floryan 2012). The first mechanism and techniques for its reduction are well understood. The second mechanism is relevant for flows over surface topographies, and the understanding of this mechanism is limited. The third mechanism has a simple physical origin, but the development of techniques for its reduction represents a significant challenge. This reduction can be achieved either directly by rearranging the form of the flow or indirectly by delaying the

† Email address for correspondence: mfloryan@eng.uwo.ca
‡ Present address: Department of Mechanical and Aerospace Engineering, Princeton University, Princeton, NJ 08544, USA.

laminar–turbulent transition. The desired change must come from altering the form of the fluid layer adjacent to the solid wall, and this can be accomplished by either passive or active means. The commonly explored techniques include changing the wall topography, applying suction/blowing or relying on plasma-, sound- or piezo-driven actuators.

This work is focused on the development of techniques for reduction of the laminar shear drag. It had been believed that reduction of this drag is not possible (Choi, Moin & Kim 1991; Chu & Karniadakis 1993), as any changes in surface topography increase the wetted area exposed to friction, which must be more than balanced by the reduction of shear. At present there are three techniques that can achieve this goal. In the first one, the use of properly structured grooves leads to changes in the bulk flow which reduce the shear sufficiently to overcome the associated increase of surface area exposed to friction (Mohammadi & Floryan 2013*a*). The groove shapes can be optimized (Mohammadi & Floryan 2013*b*), with the optimal groove having a universal shape which depends on the constraints used. In the case of grooves with equal height and depth the universal shape has a trapezoidal form while in the case of grooves with different depth and height it has a Gaussian shape.

The second technique relies on the superhydrophobic effect (Rothstein 2010). The surface topography traps gas bubbles in micropores and, thus, replaces the shear between the liquid stream and the solid wall with a shear between the stream and the gas in the bubbles. This effect is active in two-phase systems and its effectiveness depends on the hydrophobicity of the liquid and surface material and details of the surface topography. The effectiveness of this method can be increased by correctly shaping the surface pores (Samaha, Tafreshi & Gad-el-Hak 2011) and by increasing hydrophobicity through changes in surface chemistry (Quéré 2008; Reyssat, Yeomans & Quéré 2008; Zhou *et al.* 2011). The occurrence of laminar drag reduction has been demonstrated by Ou, Perot & Rothstein (2004), Ou & Rothstein (2005), Joseph *et al.* (2006) and Truesdell *et al.* (2006) among others. It is uncertain how the surface topography interacts with the pressure field, but experimental measurements demonstrate an overall drag reduction.

The third technique relies on spatially distributed heating; this creates a buoyancy field which, in turn, generates separation bubbles. The bubbles isolate the stream from direct contact with the bounding walls. Motion inside the bubbles is supported by the horizontal density gradients; these provide an additional propulsive force which reduces the required pressure gradient. This effect, sometimes referred to as the superthermohydrophobic effect (Floryan 2012), is active in single-phase fluids and is independent of surface topography. It remains effective for very small Reynolds numbers (Hossain, Floryan & Floryan 2012), since stronger flows wash the separation bubbles away, and, thus, it is relevant for applications in narrow conduits. The main objective of this analysis is to identify means for increasing the effectiveness of this effect by exploring different heating conditions. In particular, we focus our attention on the gains associated with the use of a combination of uniform and spatially modulated heating components. A model problem and the relevant formulation are discussed in § 2. The solution method is described in § 3. Properties of the long-wavelength heating are discussed in § 4. Characteristics of the short-wavelength heating are described in § 5. Heating with an arbitrary wavenumber is discussed in § 6 with detailed results presented for the Prandtl number $Pr = 0.71$, which well approximates the properties of air. In particular, the effects of the strength of the external stream are described in § 6.1, the effects of the heating conditions are presented in § 6.2 and the energy fluxes are discussed in § 6.3. Section 7 gives a short summary of the main conclusions.

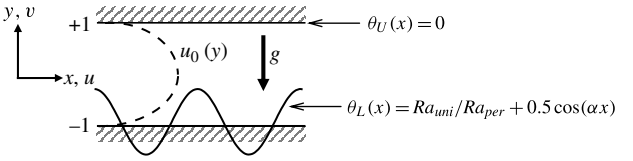

FIGURE 1. Sketch of the system configuration.

2. Problem formulation

Consider steady two-dimensional flow of a fluid confined in a channel bounded by two parallel walls extending to $\pm\infty$ in the x direction (horizontal direction) and placed a distance $2h$ apart with the gravitational acceleration g acting in the negative y direction (vertical direction), as shown in figure 1. The flow is driven in the positive x direction by a pressure gradient. The fluid is incompressible and Newtonian with thermal conductivity k, specific heat c, thermal diffusivity $\kappa = k/\rho c$, kinematic viscosity ν, dynamic viscosity μ, thermal expansion coefficient Γ and variations of the density ρ that follow the Boussinesq approximation. The flow is modified by subjecting the lower wall to a spatially distributed heating, resulting in wall temperatures of the form

$$\theta_L(x) = \sum_{n=-\infty}^{n=+\infty} \theta_L^{(n)} \mathrm{e}^{\mathrm{i}n\alpha x}, \quad \theta_U(x) = 0, \tag{2.1a,b}$$

where θ denotes the difference between the actual temperature and the temperature of the upper wall, $\theta = T - T_U$, T denotes the absolute temperature, $\theta_L^{(n)} = \theta_L^{(-n)*}$ are the reality conditions, stars denote complex conjugates, $\lambda = 2\pi/\alpha$ is the wavelength of the heating, α is its wavenumber and the subscripts L and U refer to the lower and upper walls respectively. The heating can be divided into the uniform heating described by $\theta_L^{(0)}$ and the spatially modulated heating described by the remaining terms in (2.1*a*). The conductive temperature field θ_0 corresponding to the above heating is, in the absence of any fluid movement, described by

$$\frac{\partial^2\theta_0}{\partial x^2} + \frac{\partial^2\theta_0}{\partial y^2} = 0, \tag{2.2}$$

subject to the boundary conditions (2.1). The solution has the form

$$\theta_0(x, y) = \frac{Ra_{uni}}{Ra_{per}}\hat{\theta}_0(y) + \hat{\hat{\theta}}_0(x, y), \tag{2.3a}$$

where

$$\hat{\theta}_0(y) = \tfrac{1}{2}(1 - y), \tag{2.3b}$$

$$\hat{\hat{\theta}}_0(x, y) = \sum_{n=-\infty, n\neq 0}^{n=+\infty} \hat{\hat{\theta}}_0^{(n)}(y)\mathrm{e}^{\mathrm{i}n\alpha x} = \sum_{n=-\infty, n\neq 0}^{n=+\infty} \left\{ \frac{1}{2}\theta_L^{(n)} \left[\frac{\cosh(n\alpha y)}{\cosh(n\alpha)} - \frac{\sinh(n\alpha y)}{\sinh(n\alpha)} \right] \right\} \mathrm{e}^{\mathrm{i}n\alpha x} \tag{2.3c}$$

and $\hat{\hat{\theta}}_0^{(n)} = \hat{\hat{\theta}}_0^{(-n)*}$ are the reality conditions. The uniform temperature component $\hat{\theta}_0$ has been scaled with the difference T_{uni} between the mean temperature of the lower wall

and the temperature of the upper wall, and the complete temperature θ_0, as well as its spatially modulated part, has been scaled with a conveniently selected temperature scale T_{per} characterizing the amplitude of the spatial modulations. The channel half-height h has been used as the length scale. The Rayleigh numbers based on the uniform and spatial modulation temperature scales are defined as $Ra_{uni} = g\Gamma h^3 T_{uni}/\nu\kappa$ and $Ra_{per} = g\Gamma h^3 T_{per}/\nu\kappa$ respectively. When the spatial modulation of the heating is limited to just one Fourier mode of the form $\theta_L(x) = \cos(\alpha x)/2$, (2.3*c*) simplifies to the form

$$\hat{\hat{\theta}}_0(x, y) = \hat{\hat{\theta}}_0^{(1)}(y)\mathrm{e}^{\mathrm{i}\alpha x} + \text{c.c.} = \frac{1}{8}\left[\frac{\cosh(\alpha y)}{\cosh(\alpha)} - \frac{\sinh(\alpha y)}{\sinh(\alpha)}\right]\mathrm{e}^{\mathrm{i}n\alpha x} + \text{c.c.}, \tag{2.3d}$$

and the amplitude of the temperature variations along the lower wall serves as the temperature scale T_{per}. In the above, c.c. stands for the complex conjugate.

The velocity and pressure fields in the absence of the heating have the form

$$\boldsymbol{v}_0(x, y) = [u_0(y), 0] = [1 - y^2, 0], \quad p_0(x, y) = -2x/Re, \tag{2.4a,b}$$

where $\boldsymbol{v}_0 = (u_0, v_0)$ denotes the velocity vector scaled with the maximum of the x-velocity U_{max}, p_0 stands for the pressure scaled with ρU_{max}^2 and the Reynolds number is defined as $Re = U_{max}h/\nu$.

The heating produces convection, and the resulting changes in the flow and temperature fields can be represented as

$$\left.\begin{aligned} u_T(x, y) = Reu_0(y) + u_1(x, y), \quad v_T(x, y) = v_1(x, y), \\ \theta_T(x, y) = Pr^{-1}\theta_0(x, y) + \theta_1(x, y), \quad p_T(x, y) = Re^2 p_0(x) + p_1(x, y). \end{aligned}\right\} \tag{2.5}$$

In the above, (u_T, v_T), p_T and θ_T denote the complete velocity, pressure and temperature fields respectively and (u_1, v_1), p_1 and θ_1 denote the velocity, pressure and temperature field modifications caused by the heating respectively. The complete velocity vector and the velocity modifications have been scaled using the convective velocity scale $U_v = \nu/h$, where $U_{max}/U_v = Re$, the pressure modifications have been scaled using ρU_v^2 and the total and convective temperatures have been scaled using the convective temperature scale T_v, where $T_v/T_{per} = Pr$, with Pr denoting the Prandtl number. The field equations for the flow and temperature modifications have the form

$$(Reu_0 + u_1)\frac{\partial u_1}{\partial x} + Rev_1\frac{\mathrm{d}u_0}{\mathrm{d}y} + v_1\frac{\partial u_1}{\partial y} = -\frac{\partial p_1}{\partial x} + \frac{\partial^2 u_1}{\partial x^2} + \frac{\partial^2 u_1}{\partial y^2}, \tag{2.6a}$$

$$\begin{aligned}(Reu_0 + u_1)\frac{\partial v_1}{\partial x} + v_1\frac{\partial v_1}{\partial y} = &-\frac{\partial p_1}{\partial y} + \frac{\partial^2 v_1}{\partial x^2} + \frac{\partial^2 v_1}{\partial y^2} + Ra_{per}\theta_1 \\ &+ Ra_{uni}Pr^{-1}\hat{\theta}_0 + Ra_{per}Pr^{-1}\hat{\hat{\theta}}_0,\end{aligned} \tag{2.6b}$$

$$(Reu_0 + u_1)\left(\frac{\partial\hat{\hat{\theta}}_0}{\partial x} + Pr\frac{\partial\theta_1}{\partial x}\right) + v_1\left(-\frac{Ra_{uni}}{2Ra_{per}} + \frac{\partial\hat{\hat{\theta}}_0}{\partial y} + Pr\frac{\partial\theta_1}{\partial y}\right) = \frac{\partial^2\theta_1}{\partial x^2} + \frac{\partial^2\theta_1}{\partial y^2}, \tag{2.6c}$$

$$\frac{\partial u_1}{\partial x} + \frac{\partial v_1}{\partial y} = 0. \tag{2.6d}$$

The spatially modulated heating generates convection regardless of its intensity. It is assumed that the uniform heating is weak enough that it is unable to create convection on its own; it contributes to the overall motion through (2.6*c*) and, since the system is nonlinear, prediction of the form of the resulting convection requires detailed analysis. The reader may note the presence of another term associated with the uniform heating in (2.6*b*), but this term can be omitted as it contributes only to the formation of the vertical pressure gradient. We shall keep this term for the time being as it improves the clarity of the presentation.

The main goal of the analysis is the determination of the mean pressure modification p_1, as it provides information about the ability of the heating to change the flow pressure losses. The physical problem of the determination of pressure losses is posed as the question of finding the additional pressure gradient that is required in order to maintain the same flow rate in the heated and isothermal channels. The equality of flow rates is imposed through the flow rate constraint of the form

$$Q = \int_{-1}^{1} u_T \mathrm{d}y = \int_{-1}^{1} (Reu_0 + u_1)\mathrm{d}y = 4Re/3. \tag{2.7}$$

Elimination of the imposed flow corresponds to the limit $Re \to 0$. Elimination of the heating results in $u_1 = v_1 = p_1 = \theta_1 = 0$, with the flow field being described by (2.2). This corresponds to the limit $Ra_{per} \to 0$, although the temperature scaling would have to be adjusted in order to avoid an artificial singularity in (2.3*a*). It is assumed in the further analysis that Ra_{per} is never zero, as the primary effect leading to drag reduction is associated with spatial temperature variations.

Selection of system parameters suitable for the analysis requires care due to the ease with which secondary flows can be induced. In general, such flows are expected to increase pressure losses and, thus, should be avoided. It has been found in this analysis that this is not always the case; under some conditions systems with secondary flows produced greater drag reduction than systems without secondary flows. An increase of Re increases the mixed convection and this could, eventually, lead to shear-driven instabilities; the Re values of interest in this analysis are small enough that such instabilities do not occur (Orszag 1971). The uniform heating could lead to a secondary flow through buoyancy-driven instability (Rayleigh–Bénard or RB mechanism; Chandrasekhar (1961)); the critical value of Ra_{uni} required for the onset of such convection in the absence of both forced flow and periodic heating is $Ra_{uni} = 213.5$. Freund, Pesch & Zimmermann (2011) have demonstrated that the addition of a small-amplitude periodic heating generally decreases the Ra_{uni} required for the onset. Larger values of Ra_{per} are expected to activate the spatial parametric resonance in addition to the RB mechanism, but such a situation is yet to be studied. Hossain & Floryan (2013) demonstrated that the spatially periodic heating can, by itself, lead to an instability, which is driven either by the RB mechanism or by the spatial parametric resonance. The addition of a forced flow and removal of the spatially modulated heating maintains the same critical conditions as for the uniform heating, i.e. $Ra_{uni} = 213.5$ (Gage & Reid 1968). The conditions leading to the onset of secondary flows when all these effects are present have yet to be determined. The small magnitudes of Ra_{per} and Ra_{uni} considered in this analysis minimize the potential for the formation of secondary flows. Since the conditions leading to the onset are yet to be determined, extreme care needs to be exercised when interpreting the results.

The problem formulation is closed by specifying the no-slip, no-penetration and thermal boundary conditions at the bounding walls, which have the form

$$u_1(\pm 1) = 0, \quad v_1(\pm 1) = 0, \quad \theta_1(\pm 1) = 0. \tag{2.8a–c}$$

The solution of (2.6)–(2.8) results in the determination of the velocity, temperature and pressure fields, including the mean pressure gradient, which is the main interest.

3. Method of solution

We define the stream function $\psi(x, y)$ in the usual manner, i.e. $u_1 = \partial\psi/\partial y$, $v_1 = -\partial\psi/\partial x$, and assume the solution to be of the form

$$\psi(x, y) = \sum_{n=-\infty}^{n=+\infty} \varphi^{(n)}(y) \mathrm{e}^{\mathrm{i}n\alpha x}, \quad \theta_1(x, y) = \sum_{n=-\infty}^{n=+\infty} \phi^{(n)}(y) \mathrm{e}^{\mathrm{i}n\alpha x}, \tag{3.1a,b}$$

where $\varphi^{(n)} = \varphi^{(-n)*}$ and $\phi^{(n)} = \phi^{(-n)*}$ are the reality conditions. Substitution of (3.1) into the field equations, elimination of pressure and separation of Fourier components result in the following system of ordinary differential equations for the modal functions:

$$\begin{aligned} &\mathrm{D}_n^2\varphi^{(n)} - \mathrm{i}n\alpha Re(u_0\mathrm{D}_n - \mathrm{D}^2u_0)\varphi^{(n)} - \mathrm{i}n\alpha Ra_{per}\phi^{(n)} - \mathrm{i}n\alpha Ra_{per}Pr^{-1}\hat{\hat{\theta}}_0^{(n)} \\ &\quad - \mathrm{i}\alpha \sum_{m=-\infty}^{m=+\infty} [\mathrm{D}\varphi^{(n-m)} m\mathrm{D}_m\varphi^{(m)} - (n-m)\varphi^{(n-m)}\mathrm{D}_m(\mathrm{D}\varphi^{(m)})] = 0, \end{aligned} \tag{3.2}$$

$$\begin{aligned} &\mathrm{D}_n\phi^{(n)} - \mathrm{i}n\alpha PrReu_0\phi^{(n)} - \mathrm{i}n\alpha Reu_0\hat{\hat{\theta}}_0^{(n)} - \mathrm{i}n\alpha\frac{Ra_{uni}}{2Ra_{per}}\varphi^{(n)} \\ &\quad - \sum_{m=-\infty}^{m=+\infty} \Big[\mathrm{i}\alpha(n-m)(\hat{\hat{\theta}}_0^{(n-m)} + Pr\phi^{(n-m)})\mathrm{D}\varphi^{(m)} \\ &\quad - \mathrm{i}m\alpha\varphi^{(m)}\mathrm{D}(\hat{\hat{\theta}}_0^{(n-m)} + Pr\phi^{(n-m)})\Big] = 0, \end{aligned} \tag{3.3}$$

where $\mathrm{D} = \mathrm{d}/\mathrm{d}y$, $\mathrm{D}_n = \mathrm{D}^2 - n^2\alpha^2$, $\mathrm{D}_n^2 = \mathrm{D}^4 - 2n^2\alpha^2\mathrm{D}^2 + n^4\alpha^4$, $-\infty < n < +\infty$. The relevant boundary conditions have the form

$$\mathrm{D}\varphi^{(n)}(\pm 1) = 0, \quad \varphi^{(n)}(\pm 1) = 0, \quad \phi^{(n)}(\pm 1) = 0, \tag{3.4a–c}$$

and account for the flow rate constraint.

Expansions (3.1) are truncated after a finite number of terms N_M, resulting in a system of $2(2N_M + 1)$ equations of type (3.2) and (3.3) which are solved using the variable-step-size finite-difference discretization based on the Simpson method with deferred corrections (Kierzenka & Shampine 2001, 2008). The resulting algebraic system is solved using a simplified Newton (chord) method with residual control. Selection of the number and distribution of the grid points is carried out automatically to meet the specified error bounds. The number of Fourier modes used in the solution has been selected through numerical experiments to guarantee at least six digits accuracy.

In the postprocessing stage, the velocity field is evaluated according to the relations

$$u_1(x, y) = \sum_{n=-\infty}^{n=+\infty} u_1^{(n)}(y)\mathrm{e}^{\mathrm{i}n\alpha x} = \sum_{n=-\infty}^{n=+\infty} \mathrm{D}\varphi^{(n)}(y)\mathrm{e}^{\mathrm{i}n\alpha x}, \tag{3.5a}$$

$$v_1(x, y) = \sum_{n=-\infty}^{n=+\infty} v_1^{(n)}(y)\mathrm{e}^{\mathrm{i}n\alpha x} = -\sum_{n=-\infty}^{n=+\infty} \mathrm{i}\alpha\varphi^{(n)}(y)\mathrm{e}^{\mathrm{i}n\alpha x}. \tag{3.5b}$$

The pressure field is described by

$$p_1(x, y) = Ax + \sum_{n=-\infty}^{n=+\infty} p_1^{(n)}(y)\mathrm{e}^{\mathrm{i}n\alpha x}, \tag{3.6}$$

where A represents the pressure gradient change induced by the heating, and positive values correspond to drag reduction. The pressure gradient correction A can be computed on the basis of (3.2) written for mode zero, which can be brought to the following form

$$\mathrm{D}^4\varphi^{(0)} = \sum_{n=-\infty}^{n=+\infty} \mathrm{D}^2(\mathrm{i}n\alpha\varphi^{(-n)}\mathrm{D}\varphi^{(n)}). \tag{3.7}$$

Double integration and application of the boundary conditions yield an explicit relation for A of the form

$$A = \tfrac{1}{2}[\mathrm{D}^2\varphi^{(0)}(1) - \mathrm{D}^2\varphi^{(0)}(-1)], \tag{3.8}$$

which can be readily evaluated. Another method can be derived by substituting (3.5) and (3.6) into (2.6*a*) and extracting mode zero to arrive at

$$\mathrm{D}^2u_1^{(0)} = \mathrm{D}g + A, \tag{3.9a}$$

where

$$g(y) = \sum_{n=-\infty}^{n=+\infty} v_1^{(-n)}u_1^{(n)}. \tag{3.9b}$$

Double integration and use of the boundary conditions and the flow rate constraint lead to

$$A = \tfrac{3}{2}(K_1 - K_2), \tag{3.10}$$

where

$$K_1 = \int_{-1}^{1} f(y)\mathrm{d}y, \quad K_2 = \int_{-1}^{1} g(y)\mathrm{d}y, \quad f(y) = \int_{-1}^{y} g(\eta)\mathrm{d}\eta. \tag{3.11a–c}$$

In the above, $g(y)$ is referred to as the Reynolds stress function resulting from the integration of this stress over one wavelength in the x direction, K_2 represents the result of the subsequent integration across the channel and K_1 results from the repetition of the same integration process. Equation (3.10) demonstrates that changes in the pressure gradient are associated with the Reynolds stress field created by the natural convection and modified by the stream forced to flow through the channel. Here, $A = 0$ if the phase difference between $v_1^{(n)}$ and $u_1^{(n)}$ is $\pi/2$. The maximum of

A is reached when $v_1^{(n)}$ and $u_1^{(n)}$ are in phase. When $Re = 0$, analysis of (3.2) and (3.3) demonstrates that $\varphi^{(n)}$ is imaginary, $\phi^{(n)}$ is real, $u_1^{(n)}$ is imaginary, $v_1^{(n)}$ is real and, thus, $A = 0$. A non-zero value of Re is essential for the creation of the phase difference, i.e. the modifications of the Reynolds stress field by the external stream are essential for the creation of a non-zero A. Elimination of the spatially modulated part of the heating ($Ra_{per} \to 0$) eliminates $v_1^{(n)}$ and $u_1^{(n)}$ and, thus, eliminates any change in the pressure gradient. In the analysis, the pressure gradient correction has been computed using both (3.8) and (3.11) as part of the verification of the accuracy of the numerical solution.

The total mean pressure gradient is represented as

$$\left.\frac{\partial p_T}{\partial x}\right|_{mean} = Re(-2 + A/Re), \tag{3.12}$$

and the effectiveness of the heating can be judged by comparing A/Re with -2.

It is useful to close this section with relations that permit evaluation of the pressure modal functions. Relations obtained from the x-momentum equation have the form

$$p_1^{(n)} = Reu_0u_1^{(n)} - \frac{\mathrm{i}}{n\alpha}Re\mathrm{D}u_0v_1^{(n)} - \mathrm{i}n\alpha u_1^{(n)} + \frac{\mathrm{i}}{n\alpha}\mathrm{D}^2u_1^{(n)} + \sum_{m=-\infty}^{m=+\infty}\left(\frac{n-m}{n}u_1^{(m)}u_1^{(n-m)} - \frac{\mathrm{i}}{n\alpha}\mathrm{D}u_1^{(m)}v_1^{(n-m)}\right), \quad n \neq 0. \tag{3.13a}$$

The relation for $p_1^{(0)}$ comes from the y-momentum equation and has the form

$$p_1^{(0)} = -\sum_{n=-\infty}^{n=+\infty}|v_1^{(n)}|^2 + Ra_{per}\int\phi^{(0)}\mathrm{d}y + \frac{Ra_{uni}}{Pr}\frac{y}{2}\left(1-\frac{y}{2}\right) + \text{const.} \tag{3.13b}$$

4. Long-wavelength heating ($\alpha \to 0$)

We begin assessing the importance of the uniform heating by focusing our attention on a situation where the complete heating consists of a combination of uniform heating and spatially modulated heating whose distribution is described by just one Fourier component, e.g. (2.3d). Because of the large number of parameters, we shall use asymptotic methods to identify the parameter ranges where a meaningful drag reduction can be achieved. We start this process by considering the long-wavelength limit of the spatially modulated heating, i.e. $\alpha \to 0$. In the limit the periodic part of the conductive temperature field can be approximated as

$$\hat{\hat{\theta}}_0(x, y) = \left[\hat{\hat{\theta}}_{00}(y) + \alpha^2\hat{\hat{\theta}}_{02}(y) + \alpha^4\hat{\hat{\theta}}_{04}(y) + 0(\alpha^6)\right]\cos X, \tag{4.1}$$

where definitions of $\hat{\hat{\theta}}_{00}, \hat{\hat{\theta}}_{02}, \hat{\hat{\theta}}_{04}$ are given in appendix A and $X = \alpha x$ denotes the slow scale. The field equations with x replaced by the slow scale and with the uniform heating component taken out of the y-momentum equation (see § 2) assume the form

$$\alpha(Reu_0 + u_1)\frac{\partial u_1}{\partial X} + Rev_1\frac{\mathrm{d}u_0}{\mathrm{d}y} + v_1\frac{\partial u_1}{\partial y} = -\alpha\frac{\partial p_1}{\partial X} + \alpha^2\frac{\partial^2 u_1}{\partial X^2} + \frac{\partial^2 u_1}{\partial y^2}, \tag{4.2a}$$

$$\alpha(Reu_0+u_1)\frac{\partial v_1}{\partial X}+v_1\frac{\partial v_1}{\partial y}=-\frac{\partial p_1}{\partial y}+\alpha^2\frac{\partial^2 v_1}{\partial X^2}+\frac{\partial^2 v_1}{\partial y^2}+Ra_{per}\theta_1+Ra_{per}Pr^{-1}\hat{\hat{\theta}}_0, \tag{4.2b}$$

$$(Reu_0+u_1)\left(\alpha\frac{\partial\hat{\hat{\theta}}_0}{\partial X}+Pr\alpha\frac{\partial\theta_1}{\partial X}\right)+v_1\left(-\frac{Ra_{uni}}{2Ra_{per}}+\frac{\partial\hat{\hat{\theta}}_0}{\partial y}+Pr\frac{\partial\theta_1}{\partial y}\right)=\alpha^2\frac{\partial^2\theta_1}{\partial X^2}+\frac{\partial^2\theta_1}{\partial y^2}, \tag{4.2c}$$

$$\alpha\frac{\partial u_1}{\partial X}+\frac{\partial v_1}{\partial y}=0, \tag{4.2d}$$

and lead to a solution that can be represented as

$$[u_1(X,y),\,v_1(X,y),\,\theta_1(X,y)]=\sum_{n=1}^{4}\alpha^n[U_n(X,y),\,V_n(X,y),\,\Theta_n(X,y)]+O(\alpha^5), \tag{4.3a}$$

$$p_1(X,y)=\sum_{n=0}^{3}\alpha^n P_n(X,y)+O(\alpha^4). \tag{4.3b}$$

The above expansions are substituted into (4.2), with the leading-order system being of the form

$$\frac{\partial^2 U_1}{\partial y^2}=\frac{\partial P_0}{\partial X},\quad \frac{\partial P_0}{\partial y}=\frac{Ra_{per}}{Pr}\hat{\hat{\theta}}_{00}\cos X, \tag{4.4a,b}$$

$$\frac{\partial U_1}{\partial X}+\frac{\partial V_2}{\partial y}=0,\quad \frac{\partial^2\Theta_1}{\partial y^2}=-Reu_0\hat{\hat{\theta}}_{00}\sin X, \tag{4.4c,d}$$

supplemented with the proper boundary conditions and the flow rate constraint. The solution of (4.4*a*,*b*) gives U_1 and P_0, (4.4*c*) gives V_2 and (4.4*d*) gives Θ_1 of the form

$$U_1(X,y)=Ra_{per}Pr^{-1}F_{U1}(y)\sin X,\quad V_2(X,y)=Ra_{per}Pr^{-1}F_{V2}(y)\cos X, \tag{4.5a,b}$$

$$P_0(X,y)=Ra_{per}Pr^{-1}F_{P0}(y)\cos X,\quad \Theta_1(X,y)=ReF_{\Theta 1}(y)\sin X, \tag{4.5c,d}$$

with the definitions of F_{U1}, F_{V2}, F_{P0}, $F_{\Theta 1}$ given in appendix A. Here, U_1, V_2 and P_0 describe the natural convection, which is unaffected by the forced convection at this level of approximation, and Θ_1 describes modifications of the temperature field created by the forced convection. The heating is unable to affect the mean streamwise pressure gradient. The next-order system has the form

$$\frac{\partial^2 U_2}{\partial y^2}=\frac{\partial P_1}{\partial X}+Re\left(u_0\frac{\partial U_1}{\partial X}+\frac{\mathrm{d}u_0}{\mathrm{d}y}V_2\right),\quad \frac{\partial P_1}{\partial y}=Ra_{per}\Theta_1, \tag{4.6a,b}$$

$$\frac{\partial U_2}{\partial X}+\frac{\partial V_3}{\partial y}=0,\quad \frac{\partial^2\Theta_2}{\partial y^2}=RePru_0\frac{\partial\Theta_1}{\partial X}-\hat{\hat{\theta}}_{00}U_1\sin X-\frac{Ra_{uni}}{2Ra_{per}}V_2+\frac{\partial\hat{\hat{\theta}}_{00}}{\partial y}V_2\cos X. \tag{4.6c,d}$$

A similar solution process leads to

$$U_2(X,y)=Ra_{per}Re[F_{U21}(y)+Pr^{-1}F_{U22}(y)]\cos X, \tag{4.7a}$$

$$V_3(X,y)=Ra_{per}Re[F_{V31}(y)+Pr^{-1}F_{V32}(y)]\sin X, \tag{4.7b}$$

$$P_1(X,y) = Ra_{per}Re\left[F_{P1}(y) - \tfrac{1}{1050}Pr^{-1}\right]\sin X, \tag{4.7c}$$

$$\Theta_2(X,y) = Ra_{per}Pr^{-1}F_{\Theta 21}(y) + [Ra_{uni}Pr^{-2}F_{\Theta 22}(y) + Re^2PrF_{\Theta 23}(y)]\cos X + Ra_{per}Pr^{-1}F_{\Theta 24}(y)\cos(2X), \tag{4.7d}$$

with the definitions of F_{U21}, F_{U22}, F_{V31}, F_{V32}, F_{P1}, $F_{\Theta 21}$, $F_{\Theta 22}$, $F_{\Theta 23}$, $F_{\Theta 24}$ given in appendix A. Here, F_{U21}, F_{V31} and F_{P1} arise because of temperature changes created by the forced convection, F_{U22}, F_{V32}, F_{P1} arise because of the interaction of the natural and forced convective motions, $F_{\Theta 23}$ accounts for the temperature changes created by the forced convection and $F_{\Theta 21}$, $F_{\Theta 22}$, $F_{\Theta 24}$ account for changes in the conductive temperature field created by the natural convection. The heating is still unable to generate any change in the pressure gradient and, thus, one needs to look at the next-order system, which has the form

$$\frac{\partial^2 U_3}{\partial y^2} = \frac{\partial P_2}{\partial X} + Re\left(u_0\frac{\partial U_2}{\partial X} + \frac{\mathrm{d}u_0}{\mathrm{d}y}V_3\right) + U_1\frac{\partial U_1}{\partial X} + V_2\frac{\partial U_1}{\partial y} - \frac{\partial^2 U_1}{\partial X^2}, \tag{4.8a}$$

$$\frac{\partial P_2}{\partial y} = \frac{\partial^2 V_2}{\partial y^2} + Ra_{per}\Theta_2 + Ra_{per}Pr^{-1}\hat{\hat{\theta}}_{02}\cos X, \tag{4.8b}$$

$$\frac{\partial U_3}{\partial X} + \frac{\partial V_4}{\partial y} = 0, \tag{4.8c}$$

$$\frac{\partial^2 \Theta_3}{\partial y^2} = RePru_0\frac{\partial \Theta_2}{\partial X} - Reu_0\hat{\hat{\theta}}_{02}\sin X + PrU_1\frac{\partial \Theta_1}{\partial X} - U_2\hat{\hat{\theta}}_{00}\sin X + PrV_2\frac{\partial \Theta_1}{\partial y} - \frac{Ra_{uni}}{2Ra_{per}}V_3 + \frac{\partial \hat{\hat{\theta}}_{00}}{\partial y}V_3\cos X - \frac{\partial^2 \Theta_1}{\partial X^2}. \tag{4.8d}$$

All forcing terms are purely periodic and, thus, no pressure gradient correction can be generated. It is sufficient to consider only the x-momentum equation at the next level of approximation, which takes the form

$$\frac{\partial^2 U_4}{\partial y^2} = \frac{\partial P_3}{\partial X} + Re\left(u_0\frac{\partial U_3}{\partial X} + \frac{\mathrm{d}u_0}{\mathrm{d}y}V_4\right) - \frac{\partial^2 U_2}{\partial X^2} + U_1\frac{\partial U_2}{\partial X} + U_2\frac{\partial U_1}{\partial X} + V_2\frac{\partial U_2}{\partial y} + V_3\frac{\partial U_1}{\partial y}. \tag{4.9}$$

It can be shown that only the last two terms on the right-hand side of (4.9) contribute to the aperiodic forcing, and this forcing has the form

$$FF(y) = \tfrac{1}{2}Ra_{per}^2RePr^{-1}\left\{\mathrm{D}F_{U1}(y)[F_{V31}(y) + Pr^{-1}F_{V32}(y)] + F_{V2}(y)[\mathrm{D}F_{U21}(y) + Pr^{-1}\mathrm{D}F_{U22}(y)]\right\} \tag{4.10}$$

and generates the pressure gradient correction. The solution of (4.10) with the appropriate boundary conditions and the flow rate constraint gives the aperiodic part of U_4 and the pressure gradient correction of the form

$$U_4(y)|_{mean} = \frac{1}{2}\frac{\partial p_3}{\partial X}\Big|_{mean}(y^2-1) - \frac{1}{2}(y+1)\int_{-1}^{1}\int_{-1}^{y} FF(\eta)\mathrm{d}\eta\mathrm{d}y + \int_{-1}^{y}\int_{-1}^{\zeta} FF(\eta)\mathrm{d}\eta\mathrm{d}\zeta, \tag{4.11}$$

$$\frac{\partial p_3}{\partial X}\Big|_{mean} = -\frac{3}{2}\int_{-1}^{1}\int_{-1}^{y} FF(\eta)\mathrm{d}\eta\mathrm{d}y + \frac{3}{2}\int_{-1}^{1}\int_{-1}^{y}\int_{-1}^{\zeta} FF(\eta)\mathrm{d}\eta\mathrm{d}\zeta\mathrm{d}y. \tag{4.12}$$

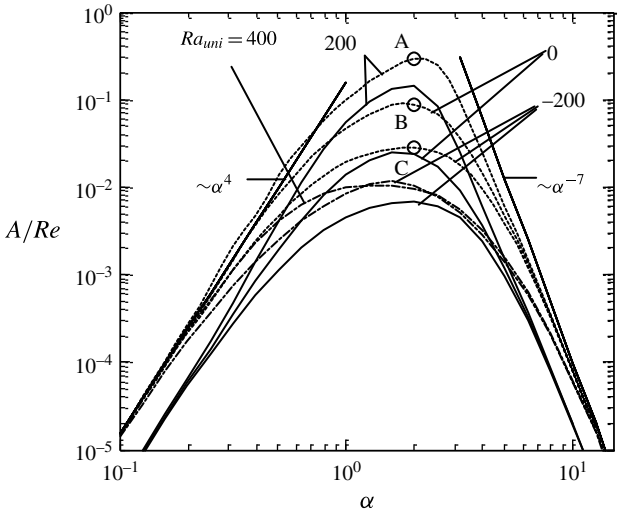

FIGURE 2. Variations of the pressure gradient correction A/Re as a function α for $Re = 1$ and $Ra_{per} = 400$ (dotted lines), $Re = 1$ and $Ra_{per} = 200$ (solid lines), $Re = 10$ and $Ra_{per} = 400$ (dashed–dotted lines) for different values of Ra_{uni}. Thin dashed lines illustrate asymptotes for small and large α. Points A, B, C correspond to $(Ra_{uni}, \Psi_{max}) = (-200, 1.5849)$, $(0, 2.2938)$, $(200, 3.8406)$ and $\alpha = 2$; the corresponding flow patterns are displayed in figure 3.

Explicit evaluations lead to the pressure gradient correction of the form

$$A = \alpha^4 Ra_{per}^2 RePr^{-1}\left(\tfrac{313}{851\,350\,500} + \tfrac{643}{2\,837\,835\,000}Pr^{-1}\right), \tag{4.13}$$

which demonstrates that it is only the periodic part of the heating that affects the overall pressure loss. The first term in the bracket arises due to the interaction between the forced and natural convection and the second one arises due to changes in the temperature field generated by the forced convection. The two effects reinforce one another. The magnitude of the drag reduction rapidly decreases when α becomes smaller and, at the same time, it increases proportionally to Ra_{per}^2 and Re. The results displayed in figure 2 demonstrate that (4.13) provides a good approximation of the drag reduction for $\alpha < 0.2$.

5. Short-wavelength heating ($\alpha \to \infty$)

We shall now turn our attention to the same heating as in the previous section but with the spatially modulated part being characterized by a very short wavelength, i.e. $\alpha \to \infty$. The periodic part of the conductive temperature field (2.3*d*) takes the form

$$\hat{\hat{\theta}}_0 = \left[\tfrac{1}{2}\mathrm{e}^{-\alpha(1+y)} + 0(\mathrm{e}^{-\alpha})\right]\cos(\alpha x). \tag{5.1}$$

The x-variations of the buoyancy force are confined to a thin boundary layer attached to the lower wall. As a result, the natural convection is confined to the same layer and, thus, all field variables above this layer can be functions of the vertical coordinate only. We shall use the method of matched asymptotic expansions to analyse the system response. The outer solution has the form

$$u_{1,outer}(x, y) = \alpha^{-7}\tilde{U}_7(y) + \alpha^{-8}\tilde{U}_8(y) + 0(\alpha^{-9}), \quad v_{1,outer}(x, y) = 0, \tag{5.2a,b}$$

$$p_{1,outer}(x,y)=\alpha^{-3}\tilde{P}_3(y)+\alpha^{-7}[\tilde{N}_7x+\tilde{P}_7(y)]+\alpha^{-8}[\tilde{N}_8x+\tilde{P}_8(y)]+0(\alpha^{-9}), \quad (5.2c)$$

$$\theta_{1,outer}(x,y)=\alpha^{-3}\tilde{\Theta}_3(y)+0(\alpha^{-7}), \quad (5.2d)$$

where the magnitudes of the relevant terms have been determined from matching with the inner solution. The results of the matching are described later in this paper. Substitution of (5.1) and (5.2) into the field equations and separation of terms of equal order of magnitude lead to the following systems:

$$\frac{\mathrm{d}^2\tilde{U}_7}{\mathrm{d}y^2}=\tilde{N}_7, \quad \frac{\mathrm{d}^2\tilde{U}_8}{\mathrm{d}y^2}=\tilde{N}_8, \quad \frac{\partial\tilde{P}_3}{\partial y}=Ra_p\tilde{\Theta}_3, \quad \frac{\mathrm{d}^2\tilde{\Theta}_3}{\mathrm{d}y^2}=0, \quad (5.3a\text{–}d)$$

whose solutions have the form

$$\tilde{\Theta}_3=\tilde{B}_3(y-1), \quad \tilde{P}_3=Ra_{per}\tilde{B}_3\left(\frac{y^2}{2}-y\right), \quad (5.4a,b)$$

$$\tilde{U}_7=\tfrac{1}{2}\tilde{N}_7(y^2-1)+\tilde{B}_7(y-1), \quad \tilde{U}_8=\tfrac{1}{2}\tilde{N}_8(y^2-1)+\tilde{B}_8(y-1). \quad (5.4c,d)$$

Constants $\tilde{B}_3$, $\tilde{B}_7$, $\tilde{B}_8$ need to be determined from matching with the inner solution, and the pressure gradient corrections $\tilde{N}_7$, $\tilde{N}_8$ need to be computed from the flow rate constraint. The heat transport has been reduced in the outer zone to vertical conduction with a non-zero boundary condition at the edge of the boundary layer created by the boundary layer phenomena. The axial flow consists of a combination of the Poiseuille and Couette components with the boundary condition at the edge of the boundary layer responsible for the selection of the required contributions from both flows.

Analysis of the boundary layer begins with the introduction of the fast scale $\xi=\alpha x$ in the horizontal direction and the stretched coordinate centred at the lower wall $\eta=\alpha(1+y)$ in the vertical direction. The externally imposed temperature and velocity fields expressed in the (ξ,η)-coordinate system have the form

$$\hat{\theta}_0=1-\alpha^{-1}\frac{\eta}{2}, \quad \hat{\hat{\theta}}_0=\frac{1}{2}\mathrm{e}^{-\eta}\cos\xi,$$

$$\frac{\partial\hat{\hat{\theta}}_0}{\partial x}=-\alpha^{-1}\frac{1}{2}\mathrm{e}^{-\eta}\sin\xi, \quad \frac{\partial\hat{\hat{\theta}}_0}{\partial y}=-\alpha^{-1}\frac{1}{2}\mathrm{e}^{-\eta}\cos\xi, \quad (5.5a)$$

$$u_0=\alpha^{-1}2\eta-\alpha^{-2}\eta^2, \quad \frac{\mathrm{d}u_0}{\mathrm{d}y}=2-\alpha^{-1}2\eta. \quad (5.5b)$$

The field equations expressed in terms of the (ξ,η)-system assume the following form:

$$\frac{\partial^2u_1}{\partial\xi^2}+\frac{\partial^2u_1}{\partial\eta^2}-\alpha^{-1}\frac{\partial p_1}{\partial\xi}=\alpha^{-1}[Re(\alpha^{-1}2\eta-\alpha^{-2}\eta^2)+u_1]\frac{\partial u_1}{\partial\xi}+\alpha^{-2}\left[Re(2-\alpha^{-1}2\eta)+\alpha\frac{\partial u_1}{\partial\eta}\right]v_1, \quad (5.6a)$$

$$\frac{\partial^2v_1}{\partial\xi^2}+\frac{\partial^2v_1}{\partial\eta^2}-\alpha^{-1}\frac{\partial p_1}{\partial\eta}=\alpha^{-1}[Re(\alpha^{-1}2\eta-\alpha^{-2}\eta^2)+u_1]\frac{\partial v_1}{\partial\xi}+\alpha^{-1}v_1\frac{\partial v_1}{\partial\eta}-\alpha^{-2}Ra_{per}\hat{\theta}_1+\alpha^{-2}\frac{1}{2}Ra_{per}Pr^{-1}\mathrm{e}^{-\eta}\cos(\xi), \quad (5.6b)$$

$$\frac{\partial u_1}{\partial \xi} + \frac{\partial v_1}{\partial \eta} = 0, \tag{5.6c}$$

$$\frac{\partial^2 \theta_1}{\partial \xi^2} + \frac{\partial^2 \theta_1}{\partial \eta^2} = \alpha^{-1}[Re(\alpha^{-1}2\eta - \alpha^{-2}\eta^2) + u_1]\left[-\frac{1}{2}\mathrm{e}^{-\eta}\sin(\xi) + Pr\frac{\partial \theta_1}{\partial \xi}\right] + \alpha^{-2}v_1\left[-\frac{Ra_{uni}}{2Ra_{per}} - \frac{1}{2}\alpha \mathrm{e}^{-\eta}\cos(\xi) + \alpha Pr\frac{\partial \theta_1}{\partial \eta}\right]. \tag{5.6d}$$

The solution of (5.6) is represented as expansions of the form

$$[u_{1,inner}(\xi,\eta), v_{1,inner}(\xi,\eta), \theta_{1,inner}(\xi,\eta)] = \sum_{n=2}^{8} \alpha^{-n}[U_n(\xi,\eta), V_n(\xi,\eta), \Theta_n(\xi,\eta)] + 0(\alpha^{-9}), \tag{5.7a}$$

$$p_{1,inner}(\xi,\eta) = \sum_{n=1}^{7} \alpha^{-n}P_n(\xi,\eta) + 0(\alpha^{-8}). \tag{5.7b}$$

Substitution of (5.7) into (5.6) and retention of the leading-order terms lead to a system of $0(\alpha^{-2})$ of the form

$$\frac{\partial^2 U_2}{\partial \xi^2} + \frac{\partial^2 U_2}{\partial \eta^2} - \frac{\partial P_1}{\partial \xi} = 0, \quad \frac{\partial^2 V_2}{\partial \xi^2} + \frac{\partial^2 V_2}{\partial \eta^2} - \frac{\partial P_1}{\partial \eta} = \frac{1}{2}Ra_{per}Pr^{-1}\mathrm{e}^{-\eta}\cos(\xi), \tag{5.8a,b}$$

$$\frac{\partial U_2}{\partial \xi} + \frac{\partial V_2}{\partial \eta} = 0, \quad \frac{\partial^2 \Theta_2}{\partial \xi^2} + \frac{\partial^2 \Theta_2}{\partial \eta^2} = -Re\eta\mathrm{e}^{-\eta}\sin(\xi). \tag{5.8c,d}$$

Its solution, which has the form

$$U_2(\xi,\eta) = -\frac{Ra_{per}}{16Pr}(2\eta - \eta^2)\mathrm{e}^{-\eta}\sin(\xi), \quad V_2(\xi,\eta) = \frac{Ra_{per}}{16Pr}\eta^2\mathrm{e}^{-\eta}\cos(\xi), \tag{5.9a,b}$$

$$P_1(\xi,\eta) = -\frac{Ra_{per}}{8Pr}(3 - 2\eta)\mathrm{e}^{-\eta}\cos(\xi), \quad \Theta_2(\xi,\eta) = \frac{Re}{4}(\eta + \eta^2)\mathrm{e}^{-\eta}\sin(\xi), \tag{5.9c,d}$$

demonstrates that the natural convection does not penetrate outside the boundary layer at this level of approximation.

The system $0(\alpha^{-3})$ has the form

$$\frac{\partial^2 U_3}{\partial \xi^2} + \frac{\partial^2 U_3}{\partial \eta^2} - \frac{\partial P_2}{\partial \xi} = 0, \quad \frac{\partial^2 V_3}{\partial \xi^2} + \frac{\partial^2 V_3}{\partial \eta^2} - \frac{\partial P_2}{\partial \eta} = 0, \tag{5.10a,b}$$

$$\frac{\partial U_3}{\partial \xi} + \frac{\partial V_3}{\partial \eta} = 0, \quad \frac{\partial^2 \Theta_3}{\partial \xi^2} + \frac{\partial^2 \Theta_3}{\partial \eta^2} = -\frac{1}{2}(-Re\eta^2 + U_2)\mathrm{e}^{-\eta}\sin(\xi) - \frac{1}{2}V_2\mathrm{e}^{-\eta}\cos(\xi), \tag{5.10c,d}$$

and leads to the following solution:

$$U_3(\xi,\eta) = 0, \quad V_3(\xi,\eta) = 0, \quad P_2(\xi,\eta) = 0, \tag{5.11a–c}$$

$$\Theta_3(\xi,\eta) = \left[\frac{Ra_{per}}{256Pr} + B_3\eta - \frac{Ra_{per}}{256Pr}(1 + 2\eta + 2\eta^2)\mathrm{e}^{-2\eta}\right] - \frac{Re}{4}\left(\frac{\eta}{2} + \frac{\eta^2}{2} + \frac{\eta^3}{3}\right)\mathrm{e}^{-\eta}\sin(\xi) + \frac{Ra_{per}}{256Pr}\left(\frac{\eta}{2} + \eta^2\right)\mathrm{e}^{-2\eta}\cos(2\xi). \tag{5.11d}$$

Equations (5.11) demonstrate that the temperature modifications are able to penetrate

outside the boundary layer as the constant B_3 needs to be determined from matching with the outer solution. The matching process results in the uniformly valid expression for the temperature of the form

$$\theta_1(x,y) = \alpha^{-3}\left\{\frac{Ra_{per}}{512Pr}(1-y) - \frac{Ra_{per}}{256Pr}[1+2\alpha(1+y)+2\alpha^2(1+y)^2]\mathrm{e}^{-2\alpha(1+y)} - \frac{Re}{4}\left[\frac{1}{2}\alpha(1+y)+\frac{1}{2}\alpha^2(1+y)^2+\frac{1}{3}\alpha^3(1+y)^3\right]\mathrm{e}^{-\alpha(1+y)}\sin(\alpha x) + \frac{Ra_{per}}{256Pr}\left[\frac{1}{2}\alpha(1+y)+\alpha^2(1+y)^2\right]\mathrm{e}^{-2\alpha(1+y)}\cos(2\alpha x)\right\} + 0(\alpha^{-5}). \quad (5.12)$$

It can be seen that the boundary layer acts as a hot wall for the outer zone.

The system $0(\alpha^{-4})$ has the form

$$\frac{\partial^2 U_4}{\partial\xi^2}+\frac{\partial^2 U_4}{\partial\eta^2}-\frac{\partial P_3}{\partial\xi} = 2\eta Re\frac{\partial U_2}{\partial\xi}+2ReV_2, \quad (5.13a)$$

$$\frac{\partial^2 V_4}{\partial\xi^2}+\frac{\partial^2 V_4}{\partial\eta^2}-\frac{\partial P_3}{\partial\eta} = -Ra_{per}\Theta_2+2\eta Re\frac{\partial V_2}{\partial\xi}, \quad (5.13b)$$

$$\frac{\partial U_4}{\partial\xi}+\frac{\partial V_4}{\partial\eta}=0, \quad \frac{\partial^2\Theta_4}{\partial\xi^2}+\frac{\partial^2\Theta_4}{\partial\eta^2} = 2RePr\eta\frac{\partial\Theta_2}{\partial\xi}-\frac{Ra_{uni}}{2Ra_{per}}V_2, \quad (5.13c,d)$$

and leads to the following solution:

$$U_4(\xi,\eta) = [Ra_{per}RePr^{-1}G_{U41}(\eta)+Ra_{per}ReG_{U42}(\eta)]\mathrm{e}^{-\eta}\cos(\xi), \quad (5.14a)$$

$$V_4(\xi,\eta) = [Ra_{per}RePr^{-1}G_{V41}(\eta)+Ra_{per}ReG_{V42}(\eta)]\mathrm{e}^{-\eta}\sin(\xi), \quad (5.14b)$$

$$P_3(\xi,\eta) = [-Ra_{per}RePr^{-1}G_{P31}(\eta)-Ra_{per}ReG_{P32}(\eta)]\mathrm{e}^{-\eta}\sin(\xi), \quad (5.14c)$$

$$\Theta_4(\xi,\eta) = [Ra_{uni}Pr^{-1}G_{\Theta41}(\eta)-Re^2PrG_{\Theta42}(\eta)]\mathrm{e}^{-\eta}\cos(\xi), \quad (5.14d)$$

where the functions G_{U41}, G_{U42}, G_{V41}, G_{V42}, G_{P31}, G_{P32}, $G_{\Theta41}$, $G_{\Theta42}$ are defined in appendix B. Free convection inside the boundary layer is unable to affect the flow and temperature fields in the outer zone at this level of approximation.

The system $0(\alpha^{-5})$ has the form

$$\frac{\partial^2 U_5}{\partial\xi^2}+\frac{\partial^2 U_5}{\partial\eta^2}-\frac{\partial P_4}{\partial\xi} = (-Re\eta^2+U_2)\frac{\partial U_2}{\partial\xi}-2\eta ReV_2+V_2\frac{\partial U_2}{\partial\eta}, \quad (5.15a)$$

$$\frac{\partial^2 V_5}{\partial\xi^2}+\frac{\partial^2 V_5}{\partial\eta^2}-\frac{\partial P_4}{\partial\eta} = -Ra_{per}\Theta_3+(-Re\eta^2+U_2)\frac{\partial V_2}{\partial\xi}+V_2\frac{\partial V_2}{\partial\eta}, \quad (5.15b)$$

$$\frac{\partial U_5}{\partial\xi}+\frac{\partial V_5}{\partial\eta}=0, \quad (5.15c)$$

$$\frac{\partial^2\Theta_5}{\partial\xi^2}+\frac{\partial^2\Theta_5}{\partial\eta^2} = 2RePr\eta\frac{\partial\Theta_3}{\partial\xi}+Pr(-Re\eta^2+U_2)\frac{\partial\Theta_2}{\partial\xi}+PrV_2\frac{\partial\Theta_2}{\partial\eta} - \frac{1}{2}\mathrm{e}^{-\eta}U_4\sin(\xi)-\frac{1}{2}\mathrm{e}^{-\eta}V_4\cos(\xi), \quad (5.15d)$$

and leads to a solution that can be expressed as

$$U_5(\xi,\eta) = \frac{Ra_{per}Re}{1920Pr}[G_{U51}(\eta)+PrG_{U52}(\eta)]\mathrm{e}^{-\eta}\cos(\xi) + \frac{Ra_{per}^2}{49\,152Pr^2}[G_{U53}(\eta)+PrG_{U54}(\eta)]\mathrm{e}^{-2\eta}\sin(2\xi), \tag{5.16a}$$

$$V_5(\xi,\eta) = \frac{Ra_{per}Re}{1920Pr}[G_{V51}(\eta)+PrG_{V52}(\eta)]\mathrm{e}^{-\eta}\sin(\xi) + \frac{Ra_{per}^2}{49\,152Pr^2}[G_{V53}(\eta)+PrG_{V54}(\eta)]\mathrm{e}^{-2\eta}\cos(2\xi), \tag{5.16b}$$

$$P_4(\xi,\eta) = -\frac{3Ra_{per}^2}{512Pr}+Ra_{per}\left(\frac{Ra_{per}\eta}{256Pr}+A_3\frac{\eta^2}{2}\right) + \frac{Ra_{per}^2}{512Pr}\left(3+4\eta+2\eta^2-\frac{\eta^4}{Pr}\right)\mathrm{e}^{-2\eta} + \frac{Ra_{per}Re}{192Pr}[G_{P41}(\eta)+PrG_{P42}(\eta)]\mathrm{e}^{-\eta}\sin(\xi) + \frac{Ra_{per}^2}{983\,040Pr^2}[G_{P43}(\eta)+PrG_{P44}(\eta)]\mathrm{e}^{-2\eta}\cos(2\xi), \tag{5.16c}$$

$$\Theta_5(\xi,\eta) = \frac{Re^2Pr}{48}G_{\Theta51}(\eta)\mathrm{e}^{-\eta}\cos(\xi) + \frac{Ra_{per}Re}{12\,288Pr}[G_{\Theta52}(\eta)+PrG_{\Theta53}(\eta)]\mathrm{e}^{-2\eta}\sin(2\xi), \tag{5.16d}$$

where the functions G_{U51}, G_{U52}, G_{U53}, G_{U54}, G_{V51}, G_{V52}, G_{V53}, G_{V54}, G_{P41}, G_{P42}, G_{P43}, G_{P44}, $G_{\Theta51}$, $G_{\Theta52}$, $G_{\Theta53}$ are given in appendix B. Equation (5.16*b*) demonstrates the appearance of vertical pressure variations outside the boundary layer which are driven by temperature $0(\alpha^{-3})$; constant A_3 has already been determined from matching of the temperature fields at $0(\alpha^{-3})$ (see (5.11*d*) and (5.12)). The pressure, expressed in terms of the outer variables, has the form

$$\begin{aligned} p_1(x,y) = {} & \alpha^{-3}\frac{Ra_{per}}{512Pr}\left(\frac{3}{2}+y-\frac{1}{2}y^2\right)+\alpha^{-4}\left\{-\frac{3Ra_{per}^2}{512Pr}+\frac{Ra_{per}^2}{512Pr}\right. \\ & \times[3+4\alpha(1+y)+2\alpha^2(1+y)^2-Pr^{-1}\alpha^4(1+y)^4]\mathrm{e}^{-2\alpha(1+y)} \\ & +\frac{Ra_{per}Re}{1920Pr^2}\left[G_{P41}(\alpha(1+y))+PrG_{P42}(\alpha(1+y))\right. \\ & \left.+Pr^2G_{P43}(\alpha(1+y))\right]\mathrm{e}^{-\alpha(1+y)}\sin(\alpha x) \\ & +\frac{Ra_{per}^2}{983\,040Pr^2}\left[G_{P44}(\alpha(1+y))\right. \\ & \left.\left.+PrG_{P45}(\alpha(1+y))\right]\mathrm{e}^{-2\alpha(1+y)}\cos(2\alpha x)\right\}. \end{aligned} \tag{5.17}$$

The system $0(\alpha^{-6})$ has the form

$$\frac{\partial^2 U_6}{\partial \xi^2}+\frac{\partial^2 U_6}{\partial \eta^2}-\frac{\partial P_5}{\partial \xi} = 2Re\eta\frac{\partial U_4}{\partial \xi}+2ReV_4, \tag{5.18a}$$

$$\frac{\partial^2 V_6}{\partial \xi^2}+\frac{\partial^2 V_6}{\partial \eta^2}-\frac{\partial P_5}{\partial \eta} = -Ra_{per}\Theta_4+2Re\eta\frac{\partial V_4}{\partial \xi}, \tag{5.18b}$$

$$\frac{\partial U_6}{\partial \xi}+\frac{\partial V_6}{\partial \eta} = 0, \tag{5.18c}$$

$$\begin{aligned}\frac{\partial^2 \Theta_6}{\partial \xi^2}+\frac{\partial^2 \Theta_6}{\partial \eta^2} &= 2RePr\eta\frac{\partial \Theta_4}{\partial \xi}+Pr(-Re\eta^2+U_2)\frac{\partial \Theta_3}{\partial \xi}\\ &\quad +PrV_2\frac{\partial \Theta_3}{\partial \eta}-\frac{1}{2}\mathrm{e}^{-\eta}U_5\sin(\xi)\\ &\quad -\frac{1}{2}\mathrm{e}^{-\eta}V_5\cos(\xi)-\frac{Ra_{uni}}{2Ra_{per}}V_4,\end{aligned} \tag{5.18d}$$

and results in the solution expressed as

$$\begin{aligned}U_6(\xi,\eta) &= \tfrac{1}{96\,160}Ra_{per}Pr^{-1}\left[Ra_{uni}G_{U61}(\eta)-Re^2G_{U62}(\eta)\right.\\ &\quad \left.-Pr^2Re^2G_{U63}(\eta)-PrRe^2G_{U64}(\eta)\right]\mathrm{e}^{-\eta}\sin(\xi),\end{aligned} \tag{5.19a}$$

$$\begin{aligned}V_6(\xi,\eta) &= -\tfrac{1}{96\,160}Ra_{per}Pr^{-1}\left[Ra_{uni}G_{V61}(\eta)+Re^2G_{V62}(\eta)\right.\\ &\quad \left.+Pr^2Re^2G_{V63}(\eta)+PrRe^2G_{V64}(\eta)\right]\mathrm{e}^{-\eta}\cos(\xi),\end{aligned} \tag{5.19b}$$

$$\begin{aligned}P_5(\xi,\eta) &= -\tfrac{1}{15\,360}Ra_{per}Pr^{-1}\left[Ra_{uni}G_{P51}(\eta)+Re^2G_{P52}(\eta)\right.\\ &\quad \left.-PrRe^2G_{P53}(\eta)+Pr^2Re^2G_{P54}(\eta)\right]\mathrm{e}^{-\eta}\cos(\xi),\end{aligned} \tag{5.19c}$$

$$\begin{aligned}\Theta_6(\xi,\eta) &= \left\{Ra_{per}^2Pr^{-2}[G_{\Theta61}(\eta)+PrG_{\Theta62}(\eta)]\mathrm{e}^{-3\eta}\right.\\ &\quad +\tfrac{1}{47\,185\,920}Pr^{-2}\left[(270-12\,645Pr)Ra_{per}^2\right.\\ &\quad \left.-B_3Pr^2Ra_{per}G_{\Theta63}(\eta)-Re^2Pr^3G_{\Theta64}(\eta)\right]\mathrm{e}^{-\eta}\Big\}\cos(\xi)\\ &\quad +Ra_{per}^2Pr^{-2}[G_{\Theta65}(\eta)+PrG_{\Theta66}(\eta)]\mathrm{e}^{-3\eta}\cos(3\xi)\\ &\quad +\left\{Re^3Pr^2G_{\Theta67}(\eta)+Ra_{uni}RePr^{-2}\left[G_{\Theta68}(\eta)\right.\right.\\ &\quad \left.\left.+PrG_{\Theta69}(\eta)\right]\right\}\mathrm{e}^{-\eta}\sin(\xi)\\ &\quad -Ra_{per}Re[G_{\Theta70}(\eta)+PrG_{\Theta71}(\eta)]\mathrm{e}^{-2\eta}\sin(2\xi),\end{aligned} \tag{5.19d}$$

which demonstrates that the boundary layer phenomena do not affect the outer zone. The functions G_{U61}, G_{U62}, G_{U63}, G_{U64}, G_{V61}, G_{V62}, G_{V63}, G_{V64}, G_{P51}, G_{P52}, G_{P53}, G_{P54}, $G_{\Theta61}$, $G_{\Theta62}$, $G_{\Theta63}$, $G_{\Theta64}$, $G_{\Theta65}$, $G_{\Theta66}$, $G_{\Theta67}$, $G_{\Theta68}$, $G_{\Theta69}$, $G_{\Theta70}$, $G_{\Theta71}$ are defined in appendix B.

The system $0(\alpha^{-7})$ has the form

$$\begin{aligned}\frac{\partial^2 U_7}{\partial \xi^2}+\frac{\partial^2 U_7}{\partial \eta^2}-\frac{\partial P_6}{\partial \xi} &= 2Re\eta\frac{\partial U_5}{\partial \xi}+(-Re\eta^2+U_2)\frac{\partial U_4}{\partial \xi}+U_4\frac{\partial U_2}{\partial \xi}+V_2\frac{\partial U_4}{\partial \eta}\\ &\quad +V_4\frac{\partial U_2}{\partial \eta}-2Re\eta V_4+2ReV_5,\end{aligned} \tag{5.20a}$$

$$\frac{\partial^2 V_7}{\partial \xi^2}+\frac{\partial^2 V_7}{\partial \eta^2}-\frac{\partial P_6}{\partial \eta} = -Ra_{per}\Theta_5+2Re\eta\frac{\partial V_5}{\partial \xi}+(-Re\eta^2+U_2)\frac{\partial V_4}{\partial \xi} + U_4\frac{\partial V_2}{\partial \xi}+V_2\frac{\partial V_4}{\partial \eta}+V_4\frac{\partial V_2}{\partial \eta}, \tag{5.20b}$$

$$\frac{\partial U_7}{\partial \xi}+\frac{\partial V_7}{\partial \eta}=0, \tag{5.20c}$$

$$\frac{\partial^2 \Theta_7}{\partial \xi^2}+\frac{\partial^2 \Theta_7}{\partial \eta^2} = 2RePr\eta\frac{\partial \Theta_5}{\partial \xi}+Pr(-Re\eta^2+U_2)\frac{\partial \Theta_4}{\partial \xi} + PrU_4\frac{\partial \Theta_2}{\partial \xi}+PrV_2\frac{\partial \Theta_4}{\partial \eta}+PrV_4\frac{\partial \Theta_2}{\partial \eta} - \frac{1}{2}e^{-\eta}U_6\sin(\xi)-\frac{1}{2}e^{-\eta}V_6\cos(\xi)-\frac{Ra_{uni}}{2Ra_{per}}V_5, \tag{5.20d}$$

and the system $0(\alpha^{-8})$ can be written as

$$\frac{\partial^2 U_8}{\partial \xi^2}+\frac{\partial^2 U_8}{\partial \eta^2}-\frac{\partial P_7}{\partial \xi} = 2Re\eta\frac{\partial U_6}{\partial \xi}+(-Re\eta^2+U_2)\frac{\partial U_5}{\partial \xi}+U_5\frac{\partial U_2}{\partial \xi} + V_2\frac{\partial U_5}{\partial \eta}+V_5\frac{\partial U_2}{\partial \eta}-2Re\eta V_5+2ReV_6, \tag{5.21a}$$

$$\frac{\partial^2 V_8}{\partial \xi^2}+\frac{\partial^2 V_8}{\partial \eta^2}-\frac{\partial P_7}{\partial \eta} = -Ra_{per}\Theta_6+2Re\eta\frac{\partial V_6}{\partial \xi}+(-Re\eta^2+U_2)\frac{\partial V_5}{\partial \xi} + U_5\frac{\partial V_2}{\partial \xi}+V_2\frac{\partial V_5}{\partial \eta}+V_5\frac{\partial V_2}{\partial \eta}, \tag{5.21b}$$

$$\frac{\partial U_8}{\partial \xi}+\frac{\partial V_8}{\partial \eta}=0, \tag{5.21c}$$

$$\frac{\partial^2 \Theta_8}{\partial \xi^2}+\frac{\partial^2 \Theta_8}{\partial \eta^2} = 2RePr\eta\frac{\partial \Theta_6}{\partial \xi}+Pr(-Re\eta^2+U_2)\frac{\partial \Theta_5}{\partial \xi} + PrU_4\frac{\partial \Theta_3}{\partial \xi}+PrU_5\frac{\partial \Theta_2}{\partial \xi}+PrV_2\frac{\partial \Theta_5}{\partial \eta} + PrV_4\frac{\partial \Theta_3}{\partial \xi}+PrV_5\frac{\partial \Theta_2}{\partial \eta}-\frac{1}{2}e^{-\eta}U_7\sin(\xi) - \frac{1}{2}e^{-\eta}V_7\cos(\xi)-\frac{Ra_{uni}}{2Ra_{per}}V_6. \tag{5.21d}$$

It is not necessary to determine complete solutions of the above systems as the mean pressure gradient correction is determined by the aperiodic components of the forcing on the right-hand sides of (5.20*a*) (RHS7) and (5.21*a*) (RHS8). These forcings have the form

$$\begin{aligned}\mathrm{RHS7}(\xi,\eta) &= -Ra_{per}^2RePr^{-2}[G_{X71}(\eta)+PrG_{X72}(\eta)]e^{-2\eta}-Ra_{per}Re^2Pr^{-1} \\ &\quad\times[G_{X73}(\eta)+PrG_{X74}(\eta)]e^{-\eta}\sin(\xi) \\ &\quad+Ra_{per}^2RePr^{-2}[G_{X75}(\eta)+PrG_{X76}(\eta)]e^{-2\eta}\cos(2\xi),\end{aligned} \tag{5.22}$$

$$\begin{aligned}\mathrm{RHS8}(\xi,\eta) &= Ra_{per}^2RePr^{-2}[G_{X81}(\eta)+PrG_{X82}(\eta)]e^{-2\eta} \\ &\quad+\{Ra_{per}RePr^{-2}Ra_{uni}G_{X83}(\eta)+Ra_{per}Re^2Pr^{-1}\end{aligned}$$

$$\times\ [G_{X84}(\eta)+PrG_{X85}(\eta)+Pr^2G_{X86}(\eta)]\big\}\,\mathrm{e}^{-2\eta}\cos(\xi)$$
$$+Ra_{per}Re^2Pr^{-2}[G_{X87}(\eta)+PrG_{X88}(\eta)]\mathrm{e}^{-2\eta}\cos(2\xi)$$
$$+\ \big\{Ra_{per}^3Pr^{-3}[G_{X89}(\eta)+PrG_{X90}(\eta)]\mathrm{e}^{-3\eta}+Ra_{per}Re^2Pr^{-1}$$
$$\times\ [G_{X91}(\eta)+PrG_{X92}(\eta)]\mathrm{e}^{-\eta}\big\}\sin(\xi)+Ra_{per}^3Pr^{-3}$$
$$\times\,[G_{X93}(\eta)+PrG_{X94}(\eta)]\mathrm{e}^{-3\eta}\sin(3\xi), \tag{5.23}$$

with the first term of (5.22) describing the aperiodic part of RHS7, i.e. $\mathrm{RHS7}_{aper}$, and the first term of (5.23) describing the aperiodic part of RHS8, i.e. $\mathrm{RHS8}_{aper}$. The functions G_{X71}, G_{X72}, G_{X73}, G_{X74}, G_{X75}, G_{X76}, G_{X81}, G_{X82}, G_{X83}, G_{X84}, G_{X85}, G_{X86}, G_{X87}, G_{X88}, G_{X89}, G_{X90}, G_{X91}, G_{X92}, G_{X93}, G_{X94} are defined in appendix B. Problems describing the aperiodic parts of U_7 and U_8, i.e. $U_{7,aper}$ and $U_{8,aper}$, have the form

$$\frac{\mathrm{d}^2U_{7,aper}}{\mathrm{d}\eta^2}=M_7+\mathrm{RHS7}_{aper},\quad U_{7,aper}(0)=0,\quad U_{7,aper}(\eta\to\infty)=\tilde{U}_{7,aper}(y\to-1), \tag{5.24a–c}$$

$$\frac{\mathrm{d}^2U_{8,aper}}{\mathrm{d}\eta^2}=M_8+\mathrm{RHS8}_{aper},\quad U_{8,aper}(0)=0,\quad U_{8,aper}(\eta\to\infty)=\tilde{U}_{8,aper}(y\to-1), \tag{5.25a–c}$$

where M_7 and M_8 stand for the unknown aperiodic parts of the streamwise pressure gradient. The solutions of (5.25*a*,*b*) and (5.26*a*,*b*) have the form

$$U_{7,aper}(\eta)=H_7+c_7\eta+M_7\frac{\eta^2}{2}+\{-H_7+Ra_{per}^2RePr^{-2}[G_{U71}(\eta)+PrG_{U72}(\eta)]\}\mathrm{e}^{-2\eta}, \tag{5.26}$$

$$U_{8,aper}(\eta)=H_8+c_8\eta+M_8\frac{\eta^2}{2}+\{-H_8+Ra_{per}^2RePr^{-2}[G_{U81}(\eta)+PrG_{U82}(\eta)]\}\mathrm{e}^{-2\eta}, \tag{5.27}$$

where the constants c_7 and c_8 are to be determined from matching, G_{U71}, G_{U72}, G_{U81}, G_{U82} are defined in appendix B and

$$H_7=\frac{(16+11Pr)Ra_{per}^2Re}{8192Pr^2},\quad H_8=-\frac{(375+180Pr)Ra_{per}^2Re}{81\,920Pr^2}. \tag{5.28a,b}$$

After matching, the aperiodic part of the velocity profile can be expressed as

$$u_{1,aper}(y)=\alpha^{-7}\left\{-\frac{\tilde{N}_7}{2}(1-y^2)+\frac{1}{2}H_7(1-y)+\big\{H_7+Ra_{per}^2RePr^{-2}\right.$$
$$\left.\times\ [G_{U71}(\alpha(1+y))+PrG_{U72}(\alpha(1+y))]\big\}\,\mathrm{e}^{-2\alpha(1+y)}\right\}$$
$$+\alpha^{-8}\left\{-\frac{\tilde{N}_8}{2}(1-y^2)+\frac{1}{2}H_8(1-y)+\big\{H_8+Ra_{per}^2RePr^{-2}\right.$$
$$\left.\times\ [G_{U81}(\alpha(1+y))+PrG_{U82}(\alpha(1+y))]\big\}\,\mathrm{e}^{-2\alpha(1+y)}\right\}, \tag{5.29}$$

and application of the flow rate constraint results in the mean pressure gradient of the

form

$$\left.\frac{\partial p_1}{\partial x}\right|_{mean} = A = \alpha^{-7}\tilde{N}_7 + \alpha^{-8}\tilde{N}_8 = \alpha^{-7}\frac{3(16+11Pr)Ra_{per}^2 Re}{16\,384Pr^2} - \alpha^{-8}\frac{27(55+32Pr)Ra_{per}^2 Re}{32\,768Pr^2} + 0(\alpha^{-9}). \tag{5.30}$$

It can be seen that the heating always reduces drag. The outer flow sees the edge of the boundary layer as a wall moving in the positive x direction. This effect is responsible for the appearance of the Couette component which carries a positive increase of the flow rate. The Poiseuille component must appear in order to compensate for this flow rate increase as the total flow rate cannot change. Equation (5.30) provides a good approximation for the drag reduction when $\alpha > 8$ (see figure 2) and demonstrates that the uniform heating plays no role when the short-wavelength heating is used.

6. Heating with wavenumbers $\alpha = 0(1)$

It has been demonstrated in the previous two sections that the uniform heating does not play any role when it is combined with spatially modulated heating characterized by either short or long wavelengths. We shall now explore heating with the wavenumbers $\alpha = 0(1)$ and focus our attention on fluids with the Prandtl number $Pr = 0.71$, which well approximates the properties of air. The results displayed in figure 2 demonstrate that a meaningful drag reduction can be achieved for such heating conditions, and an increase of the uniform heating increases the drag reduction. Hossain *et al.* (2012) studied flows exposed to spatially modulated heating with zero mean and demonstrated that the formation of separation bubbles was essential for drag reduction. This reduction occurs because (i) the bubbles reduce direct contact between the stream and the walls and thus reduce the shear that the stream is exposed to and (ii) fluid in the bubbles rotates on its own due to density differences and this process generates a propulsive force. Figure 3 illustrates the changes in the flow topology due to an increase of the uniform heating while keeping the magnitude of the modulated heating unchanged. The reference topology for the purely modulated heating ($Ra_{uni} = 0$) is displayed in figure 3(*b*) for $Ra_{per} = 400$ and $Re = 1$. The corresponding intensity of motion can be characterized in terms of the maximum of the stream function, i.e. $\psi_{max} = 2.2938$. Uniform cooling of the lower wall ($Ra_{uni} = -200$) results in a reduction of the size of the bubbles (see figure 3*a*) as well as a reduction of the intensity of the motion ($\psi_{max} = 1.5849$). Uniform heating of the same wall ($Ra_{uni} = 200$) increases the size of the bubbles (see figure 3*c*) as well as the intensity of the motion ($\psi_{max} = 3.8406$). We shall quantify these phenomena in the forthcoming discussion.

6.1. *Effects of the strength of the forced flow*

The strength of the forced flow is measured using the Reynolds number Re. It is known that for $Ra_{uni} = 0$ an increase of Re increases the intensity of this motion which, eventually, washes away the separation bubbles and, thus, eliminates the drag reducing effect (Hossain *et al.* 2012). We shall now inquire how well stronger bubbles associated with the presence of the uniform heating are able to withstand the push created by the forced motion. We begin the analysis by assuming the Reynolds number

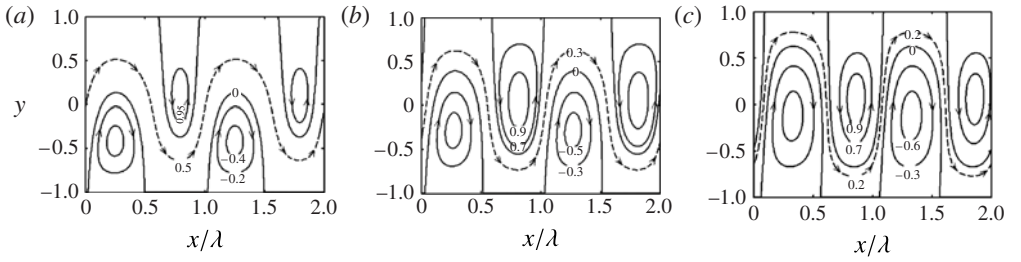

FIGURE 3. Variations of the flow topology as a function of the intensity of the uniform heating Ra_{uni} for $\alpha = 2$, $Ra_{per} = 400$, $Re = 1$. The complete stream function $\Psi(x, y) = Re(-y^3/3 + y + 2/3) + \psi(x, y)$ is normalized with its maximum Ψ_{max}. The results displayed in figure 3(*a–c*) correspond to points A, B, C in figure 2.

to be $Re \ll 1$, which leads to a representation of the solution in the following form:

$$(u_1, v_1, p_1, \Theta_1) = (u_{10}, v_{10}, p_{10}, \Theta_{10}) + Re(u_{11}, v_{11}, p_{11}, \Theta_{11}) + 0(Re^2). \tag{6.1}$$

Substitution of (6.1) into (2.6) and grouping of terms of the same order of magnitude in Re result in a sequence of systems, with the two highest-order systems having the following forms.

System $0(Re^0)$:

$$\nabla^2 u_{10} - \frac{\partial p_{10}}{\partial x} - u_{10}\frac{\partial u_{10}}{\partial x} - v_{10}\frac{\partial u_{10}}{\partial y} = 0, \tag{6.2a}$$

$$\nabla^2 v_{10} - \frac{\partial p_{10}}{\partial y} - u_{10}\frac{\partial v_{10}}{\partial x} - v_{10}\frac{\partial v_{10}}{\partial y} + Ra_{per}\theta_{10} = -Ra_{per}Pr^{-1}\hat{\hat{\theta}}_0, \tag{6.2b}$$

$$\nabla^2 \theta_{10} - v_{10}\left(-\frac{Ra_{uni}}{2Ra_{per}} + \frac{\partial \hat{\hat{\theta}}_0}{\partial y} + Pr\frac{\partial \theta_{10}}{\partial y}\right) - u_{10}\left(\frac{\partial \hat{\hat{\theta}}_0}{\partial x} + Pr\frac{\partial \theta_{10}}{\partial x}\right) = 0, \tag{6.2c}$$

$$\frac{\partial u_{10}}{\partial x} + \frac{\partial v_{10}}{\partial y} = 0. \tag{6.2d}$$

System $0(Re)$:

$$\nabla^2 u_{11} - \frac{\partial p_{11}}{\partial x} - u_{11}\frac{\partial u_{10}}{\partial x} - u_{10}\frac{\partial u_{11}}{\partial x} - v_{10}\frac{\partial u_{11}}{\partial y} - v_{11}\frac{\partial u_{10}}{\partial y} = u_0\frac{\partial u_{10}}{\partial x} + v_{10}\frac{\mathrm{d}u_0}{\mathrm{d}y}, \tag{6.3a}$$

$$\nabla^2 v_{11} - \frac{\partial p_{11}}{\partial y} + Ra_{per}\theta_{11} - u_{10}\frac{\partial v_{11}}{\partial x} - u_{11}\frac{\partial v_{10}}{\partial x} - v_{10}\frac{\partial v_{11}}{\partial y} - v_{11}\frac{\partial v_{10}}{\partial y} = u_0\frac{\partial v_{10}}{\partial x}, \tag{6.3b}$$

$$\nabla^2 \theta_{11} - u_{11}\left(\frac{\partial \hat{\hat{\theta}}_0}{\partial x} + Pr\frac{\partial \theta_{10}}{\partial x}\right) - Pru_{10}\frac{\partial \theta_{11}}{\partial x} - Prv_{10}\frac{\partial \theta_{11}}{\partial y} - v_{11}\left(-\frac{Ra_{uni}}{2Ra_{per}} + \frac{\partial \hat{\hat{\theta}}_0}{\partial y} + Pr\frac{\partial \theta_{10}}{\partial y}\right) = u_0\left(\frac{\partial \hat{\hat{\theta}}_0}{\partial x} + Pr\frac{\partial \theta_{10}}{\partial x}\right), \tag{6.3c}$$

$$\frac{\partial u_{11}}{\partial x} + \frac{\partial v_{11}}{\partial y} = 0. \tag{6.3d}$$

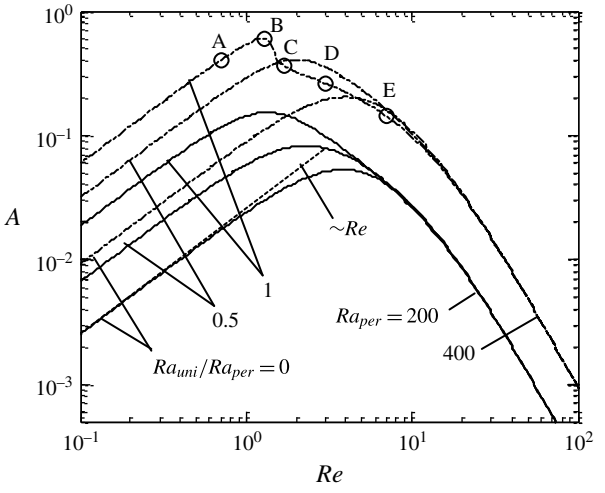

FIGURE 4. Variations of the pressure gradient correction A as a function of Re for $Ra_{per} = 200$ (solid lines) and $Ra_{per} = 400$ (dashed lines) for $\alpha = 2$. Each periodic heating is combined with the uniform heating corresponding to $Ra_{uni}/Ra_{per} = 0,\ 0.5,\ 1$. Flow topologies corresponding to points A–E are displayed in figure 5(*a–e*) respectively. The dotted line illustrates the asymptote for small Re.

The solution of (6.2) can be represented in terms of a real Fourier series of the form

$$u_{10}(x, y) = \sum_{n=0}^{\infty} \hat{u}_{10}^{(n)}(y) \sin(n\alpha x), \quad v_{10}(x, y) = \sum_{n=0}^{\infty} \hat{v}_{10}^{(n)}(y) \cos(n\alpha x), \tag{6.4a,b}$$

$$p_{10}(x, y) = \sum_{n=0}^{\infty} \hat{p}_{10}^{(n)}(y) \cos(n\alpha x), \quad \theta_{10}(x, y) = \sum_{n=0}^{\infty} \hat{\theta}_{10}^{(n)}(y) \cos(n\alpha x). \tag{6.4c,d}$$

The correctness of (6.4) can be readily verified by its substitution into (6.2). Equation (6.4) demonstrates that u_{10} and v_{10} are $\pi/2$ out of phase and, thus, the Reynolds stress function $g(y)$ defined by (3.9*b*) is always zero. This demonstrates that, not surprisingly, the pressure gradient correction is always zero when $Re = 0$. Equation (6.3) does not admit a solution in a form similar to (6.4), which, again, can be readily verified by direct substitution. The cross-product terms generate a phase shift between u_{11} and v_{11}, and this leads to a non-zero-valued function g. The pressure gradient correction is thus proportional to Re, in agreement with the results presented in figure 4. The presence of the uniform heating does not affect the functional dependence of A on Re.

The results displayed in figure 4 illustrate an initial growth of A as Re increases, followed by a rapid decrease for $Re \geqslant \sim 10$. This process is qualitatively similar for channels subject to spatially modulated heating with, as well as without, the uniform heating component. The drop in the drag reduction is associated with a change in the topology of the separation bubbles and their eventual elimination. Figure 5 illustrates this process for $Ra_{per} = 400$, $Ra_{uni}/Ra_{per} = 1$. At $Re = 0$ (not shown) the convection generates pairs of counter-rotating rolls, with the fluid moving upwards above the hot spots. At $Re = 0.7$ the rolls play the role of separation bubbles with a very narrow

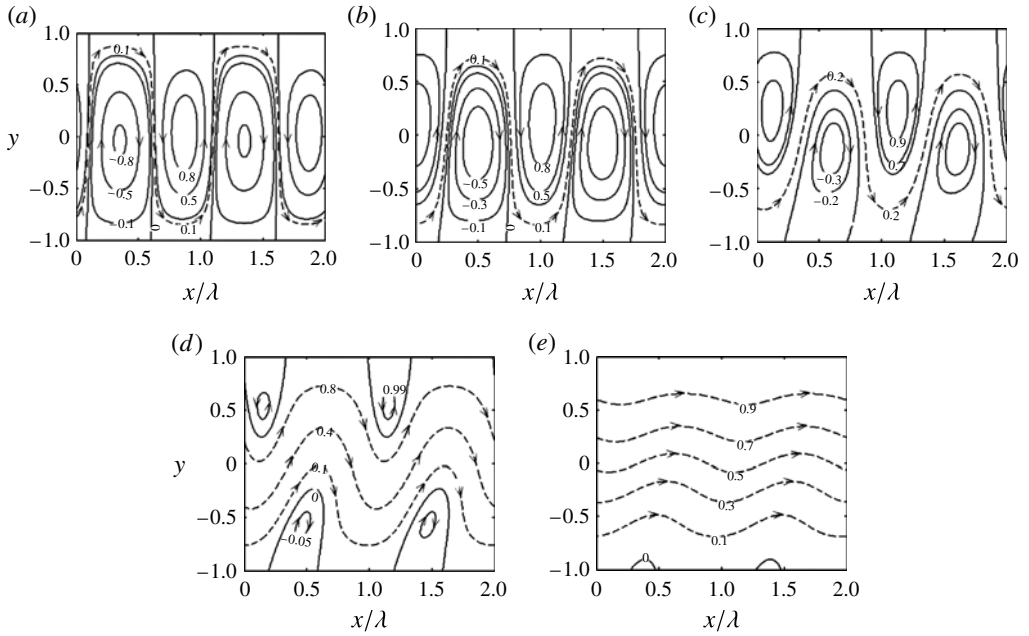

FIGURE 5. Variations of the flow topology as a function of the flow Reynolds number Re for $\alpha = 2$, $Ra_{per} = 400$, $Ra_{uni}/Ra_{per} = 1$. The complete stream function $\Psi(x, y) = Re(-y^3/3 + y + 2/3) + \psi(x, y)$ is normalized with its maximum Ψ_{max}. Figures 5(*a*)–5(*e*) correspond to $(Re, \Psi_{max}) = (0.7, 5.7263)$, (1.3, 5.1895), (1.7, 3.785), (3, 4.2603), (7, 9.333).

stream meandering between them (see figure 5*a*). The upper and lower bubbles have nearly the same size but the location of the maximum upward motion is pushed in the streamwise direction and, as a result, the locations of the separation points at the lower wall do not overlap with the temperature extrema. At $Re = 1.3$ the stream widens, the bubbles shrink and begin to tilt in the streamwise direction; at the same time the bubbles are pushed further downstream with the lower bubbles located above the cold sections of the wall (see figure 5*b*). At $Re = 1.7$ the bubbles do not move any further but begin to tilt more visibly (figure 5*c*). At $Re = 3$ the bubbles visibly shrink and the stream occupies the majority of the channel (figure 5*d*). At $Re = 7$ the bubbles are almost completely washed away (figure 5*e*). The bubble shrinking process is fairly smooth for smaller Ra_{per} (see curves for $Ra_{per} = 200$ in figure 4) and for smaller Ra_{uni}/Ra_{per} (see curves for $Ra_{uni}/Ra_{per} = 0$, 0.5) but follows a rapid rearrangement for higher Ra_{per} and Ra_{uni}/Ra_{per} (see the curve for $Ra_{per} = 400$, $Ra_{uni}/Ra_{per} = 1$ in figure 4). This rapid change is associated with the destruction of the larger bubbles formed by such heating. We shall return to this issue later in the discussion.

The late stages of the bubble elimination process can be followed analytically by noting that for large enough Re the natural convection is contained in a boundary layer that develops at the lower wall. The relevant solution can be determined using the method of matched asymptotic expansions. Details are omitted from this presentation due to their excessive length.

The results presented in figure 4 illustrate the range of variation of A that can be achieved by varying Re. A meaningful drag reduction can be achieved for $Re < 10$, and, thus, this is the range of Re that the further analysis is focused on.

6.2. *Effects of heating conditions*

We begin the analysis by assuming that the applied heating leads to a weak convection. It will be shown that it is not necessary to define the meaning of 'weak', at least at the leading order of approximation.

6.2.1. *Weak convection*

The solution is assumed to be of the form

$$(u_1, v_1, p_1, \theta_1) = \varepsilon(U_1, V_1, P_1, \Theta_1) + \varepsilon^2(U_2, V_2, P_2, \Theta_2) + 0(\varepsilon^3), \tag{6.5}$$

where $\varepsilon \ll 1$ is a measure of the strength of convection. Substitution of (6.5) into (2.6) and retention of terms of the two highest orders of magnitude lead to a system $0(\varepsilon)$ in the form

$$\nabla^2 U_1 - Reu_0 \frac{\partial U_1}{\partial x} - ReV_1 \frac{\mathrm{d}u_0}{\mathrm{d}y} - \frac{\partial P_1}{\partial x} = 0, \tag{6.6a}$$

$$\nabla^2 V_1 - Reu_0 \frac{\partial V_1}{\partial x} - \frac{\partial P_1}{\partial y} + Ra_{per}\Theta_1 = -Ra_{per}Pr^{-1}\tilde{\theta}_0, \tag{6.6b}$$

$$\nabla^2 \Theta_1 - PrReu_0 \frac{\partial \Theta_1}{\partial x} + \frac{Ra_{uni}}{2Ra_{per}} V_1 = Reu_0 \frac{\partial \tilde{\theta}_0}{\partial x}, \tag{6.6c}$$

$$\frac{\partial U_1}{\partial x} + \frac{\partial V_1}{\partial y} = 0, \tag{6.6d}$$

where $\tilde{\theta}_0 = \hat{\tilde{\theta}}_0/\varepsilon = 0(1)$, and a system $0(\varepsilon^2)$ of the form

$$\nabla^2 U_2 - Reu_0 \frac{\partial U_2}{\partial x} - ReV_2 \frac{\mathrm{d}u_0}{\mathrm{d}y} - \frac{\partial P_2}{\partial x} = U_1 \frac{\partial U_1}{\partial x} + V_1 \frac{\partial U_1}{\partial y}, \tag{6.7a}$$

$$\nabla^2 V_2 - Reu_0 \frac{\partial V_2}{\partial x} - \frac{\partial P_2}{\partial y} + Ra_{per}\Theta_2 = U_1 \frac{\partial V_1}{\partial x} + V_1 \frac{\partial V_1}{\partial y}, \tag{6.7b}$$

$$\nabla^2 \Theta_2 - PrReu_0 \frac{\partial \Theta_2}{\partial x} + \frac{Ra_{uni}}{2Ra_{per}} V_2 = U_1 \frac{\partial \tilde{\theta}_0}{\partial x} + V_1 \frac{\partial \tilde{\theta}_0}{\partial y} + PrU_1 \frac{\partial \Theta_1}{\partial x} + PrV_1 \frac{\partial \Theta_1}{\partial y}, \tag{6.7c}$$

$$\frac{\partial U_2}{\partial x} + \frac{\partial V_2}{\partial y} = 0. \tag{6.7d}$$

It can be seen that the uniform heating affects the overall system dynamics even when convection is weak. Equations (6.6) and (6.7) need to be supplemented by the homogeneous boundary conditions and constraints associated with the fixed flow rate condition.

The solution process begins with rearrangement of (6.6) into the form

$$\nabla^2 \ddot{U}_1 - Reu_0 \frac{\partial \ddot{U}_1}{\partial x} - Re\ddot{V}_1 \frac{\mathrm{d}u_0}{\mathrm{d}y} - \frac{\partial \ddot{P}_1}{\partial x} = 0, \tag{6.8a}$$

$$\nabla^2 \ddot{V}_1 - Reu_0 \frac{\partial \ddot{V}_1}{\partial x} - \frac{\partial \ddot{P}_1}{\partial y} + Ra_{per}\ddot{\Theta}_1 = -Ra_{per}Pr^{-1}\hat{\tilde{\theta}}_0, \tag{6.8b}$$

$$\nabla^2\ddot{\Theta}_1 - PrReu_0\frac{\partial\ddot{\Theta}_1}{\partial x} + \frac{Ra_{uni}}{2Ra_{per}}\ddot{V}_1 = Reu_0\frac{\partial\hat{\hat{\theta}}_0}{\partial x}, \tag{6.8c}$$

$$\frac{\partial\ddot{U}_1}{\partial x} + \frac{\partial\ddot{V}_1}{\partial y} = 0, \tag{6.8d}$$

where $\ddot{U}_1 = \varepsilon U_1$, $\ddot{V}_1 = \varepsilon V_1$, $\ddot{P}_1 = \varepsilon P_1$, $\ddot{\Theta}_1 = \varepsilon\Theta_1$. The above system can be solved without the need for an explicit identification of ε. The form of the forcing on the right-hand side of (6.6) leads to a solution of the form

$$[\ddot{U}_1(x,y), \ddot{V}_1(x,y), \ddot{P}_1(x,y), \ddot{\Theta}_1(x,y)] = [\ddot{U}_1^{(1)}(y), \ddot{V}_1^{(1)}(y), \ddot{P}_1^{(1)}(y), \ddot{\Theta}_1^{(1)}(y)]\mathrm{e}^{\mathrm{i}\alpha x} + \text{c.c.}, \tag{6.9}$$

where c.c. stands for the complex conjugate. Modal functions are defined by the solution of the following problem:

$$(\mathrm{D}^2 - \alpha^2 - \mathrm{i}\alpha Reu_0)\ddot{U}_1^{(1)} - \mathrm{i}\alpha\ddot{P}_1^{(1)} - Re\frac{\mathrm{d}u_0}{\mathrm{d}y}\ddot{V}_1^{(1)} = 0, \tag{6.10a}$$

$$(\mathrm{D}^2 - \alpha^2 - \mathrm{i}\alpha Reu_0)\ddot{V}_1^{(1)} - \mathrm{D}\ddot{P}_1^{(1)} + Ra_{per}\ddot{\Theta}_1^{(1)} = -\frac{Ra_{per}}{Pr}\hat{\hat{\theta}}_0^{(1)}, \tag{6.10b}$$

$$(\mathrm{D}^2 - \alpha^2 - \mathrm{i}\alpha PrReu_0)\ddot{\Theta}_1^{(1)} + \frac{Ra_{uni}}{2Ra_{per}}\ddot{V}_1^{(1)} = \mathrm{i}\alpha Reu_0\hat{\hat{\theta}}_0^{(1)}, \tag{6.10c}$$

$$\mathrm{i}\alpha\ddot{U}_1^{(1)} + \mathrm{D}\ddot{V}_1^{(1)} = 0, \tag{6.10d}$$

$$\ddot{U}_1^{(1)}(\pm1) = 0, \quad \ddot{V}_1^{(1)}(\pm1) = 0, \quad \ddot{\Theta}_1^{(1)}(\pm1) = 0, \tag{6.10e}$$

which needs to be solved numerically. The solution has been determined using the same technique as described in § 3. Equation (6.9) demonstrates that there is no change in the mean pressure gradient at this order of approximation.

The form of solution of the next order of approximation is dictated by the forcing on the right-hand side of (6.7). This form, which can be expressed as

$$[U_2(x,y), V_2(x,y), \Theta_2(x,y)] = \sum_{n=-2,0,2}[U_2^{(n)}(y), V_2^{(n)}(y), \Theta_2^{(n)}(y)]\mathrm{e}^{\mathrm{i}n\alpha x}, \tag{6.11a}$$

$$P_2(x,y) = \sum_{n=-2,0,2}P_2^{(n)}(y)\mathrm{e}^{\mathrm{i}n\alpha x} + A_2 x, \tag{6.11b}$$

demonstrates the appearance of both the net heat transfer between the walls and the pressure gradient correction. Substitution of (6.11) into (6.7*d*) and extraction of mode zero demonstrate that $V_2^{(0)}(y) = 0$. Substitution of (6.11) into (6.7*a*) and extraction of mode zero lead to

$$\mathrm{D}^2U_2^{(0)} - A_2 = \left(U_1\frac{\partial U_1}{\partial x} + V_1\frac{\partial U_1}{\partial y}\right)\Big|_{aperiodic\ \ part}, \tag{6.12a}$$

with the boundary conditions and the flow rate constraint of the form

$$U_2^{(0)}(\pm1) = 0, \quad \int_{-1}^{1}U_2^{(0)}\mathrm{d}y = 0. \tag{6.12b,c}$$

Equation (6.12) can be expressed in terms of variables defined by (6.9), resulting in the following form:

$$\varepsilon \mathrm{D}^2 \dddot{U}_2^{(0)} - \varepsilon \dddot{A}_2 = \dddot{V}_1^{(1)} \mathrm{D} \dddot{U}_1^{(-1)} + \dddot{V}_1^{(-1)} \mathrm{D} \dddot{U}_1^{(1)}, \quad \dddot{U}_2^{(0)}(\pm 1) = 0, \quad \int_{-1}^{1} \dddot{U}_2^{(0)} \mathrm{d}y = 0, \tag{6.13a–c}$$

where $\dddot{A}_2 = \varepsilon A_2$, $\dddot{U}_2^{(0)} = \varepsilon U_2^{(0)}$. Double integration of (6.13*a*) and application of (6.13*b*) give the correction for the mean velocity distribution of the form

$$\varepsilon \dddot{U}_2^{(0)} = -\frac{1}{2} \varepsilon \dddot{A}_2 (1 - y^2) - \frac{1}{2} \int_{-1}^{1} \dddot{g}(y) \mathrm{d}y (1 + y) + \int_{-1}^{y} \dddot{g}(\eta) \mathrm{d}\eta, \tag{6.14a}$$

$$\dddot{g}(y) = \dddot{V}_1^{(-1)} \dddot{U}_1^{(1)} + \dddot{V}_1^{(1)} \dddot{U}_1^{(-1)}, \tag{6.14b}$$

where $\dddot{g}(y)$ is the one-mode version of the Reynolds stress function $g(y)$ defined by (3.9*b*). Application of (6.13*c*) yields

$$\varepsilon \dddot{A}_2 = -\frac{3}{2} \int_{-1}^{1} \dddot{g}(y) \mathrm{d}y + \frac{3}{2} \int_{-1}^{1} \int_{-1}^{y} \dddot{g}(\eta) \mathrm{d}\eta \mathrm{d}y. \tag{6.15}$$

The pressure gradient correction can now be expressed as

$$\left. \frac{\partial p_1}{\partial x} \right|_{mean} = A = \varepsilon^2 \left. \frac{\partial P_2}{\partial x} \right|_{mean} = \varepsilon^2 A_2 = \varepsilon \dddot{A}_2 = -\frac{3}{2} \int_{-1}^{1} \dddot{g}(y) \mathrm{d}y + \frac{3}{2} \int_{-1}^{1} \int_{-1}^{y} \dddot{g}(\eta) \mathrm{d}\eta \mathrm{d}y, \tag{6.16}$$

without the need for an explicit identification of ε. The effects of the uniform heating enter the above relation implicitly as they change the form of the Reynolds stress function. The integrations appearing in (6.16) have been carried out numerically; a two-point fourth-order accurate trapezoidal rule based on the values of the function and its first derivative at the grid points has been used.

The results displayed in figure 6 demonstrate that convection can be considered to be weak only for certain combinations of Ra_{per} and Ra_{uni}. For low Ra_{per} the 'weak-convection' model accurately captures the system properties for the whole range of Ra_{uni} studied (see the curve for $Ra_{per} = 100$ in figure 6). An increase of Ra_{per} rapidly reduces the range of its applicability, e.g. when $Ra_{per} = 300$ the model can be applied only for $Ra_{uni} < 100$ (see figure 6) and when $Ra_{per} = 500$ this range decreases to $Ra_{uni} < 0$. The comparison of different curves in figure 6 illustrates significant intensification of convection due to the introduction of even a small amount of uniform heating, and an increase of the effectiveness of the uniform heating component for higher amplitudes of heating modulations.

6.2.2. *Effects of the uniform heating*

The presence of the spatially distributed heating is essential for drag reduction. In the simplest case considered in this analysis, i.e. the temperature distribution is described by (2.3*d*), the temperature of the lower wall must locally decrease/increase with respect to the temperature of the upper wall. This may lead to the need for local cooling/heating of the lower wall and this may be difficult to implement in practice. It is much simpler either to just heat the lower wall with some spatial variability added to it or to cool it in the same manner. The need for the local temperature reduction is eliminated as long as $Ra_{uni}/Ra_{per} > 0.5$. Similarly, the need for the local temperature

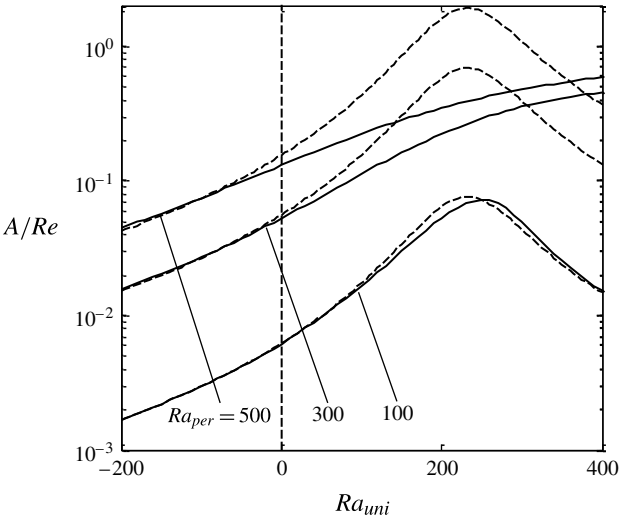

FIGURE 6. Variations of the pressure gradient correction as a function of Ra_{uni} for different magnitudes of the spatially modulated heating obtained using the 'weak-convection' approximation (dashed lines) as well as the complete model equations (solid lines) for $Re = 1$, $\alpha = 2$.

increase is eliminated if $Ra_{uni}/Ra_{per} < -0.5$. The analysis given in appendix C predicts that the pressure gradient correction changes proportionally to the magnitude of the uniform heating as long as this heating deviates slightly from the reference case of sinusoidal heating. The results presented in figure 6 demonstrate that such an approximation is unable to capture the system behaviour under conditions that are of interest in applications, i.e. for $Ra_{uni}/Ra_{per} > 0.5$ and for $Ra_{uni}/Ra_{per} < -0.5$. In this range of parameters one must rely on the numerical method described in § 3. This method matches the limiting cases as demonstrated in figures 2, 4 and 6, and this increases the level of confidence in the numerical results.

The results displayed in figure 6 demonstrate a decrease of the drag reducing effect when the mean temperature of the lower wall is reduced below the temperature of the upper wall ($Ra_{uni} < 0$). The effectiveness of drag reduction increases for $Ra_{uni} > 0$ and, thus, such heating conditions are of the main interest, especially for $Ra_{uni}/Ra_{per} > 0.5$.

The drag reduction that can be achieved using combinations of spatially modulated and spatially uniform heating components is illustrated in figure 7, which displays variations of A/Re as a function of Ra_{per}. In figure 7(a) the strength of the uniform heating is expressed as a fraction of the modulated heating, i.e. Ra_{uni}/Ra_{per}, which permits simple identification of the conditions when the lower wall has a mean temperature higher ($Ra_{uni}/Ra_{per} > 0.5$) or lower ($Ra_{uni}/Ra_{per} < -0.5$) than that of the upper wall. It can be seen that the use of uniform cooling decreases the drag reduction in the whole range of Ra_{uni} studied when compared with the reference case of $Ra_{uni} = 0$, while uniform heating leads to a significant increase of the drag reduction. Increases of the order of 300 % can be achieved with $Ra_{uni}/Ra_{per} \leqslant 0.5$ in the whole range of Ra_{per} considered. Higher gains are possible for $Ra_{uni}/Ra_{per} > 0.5$ but they are limited by the appearance of secondary states. These states may either coexist with the primary states (see the curves for $Ra_{uni}/Ra_{per} = 0.8$, 1, 1.2 in figure 7a) or may eliminate these states (see the curves for $Ra_{uni}/Ra_{per} = 1.5$, 1.7,

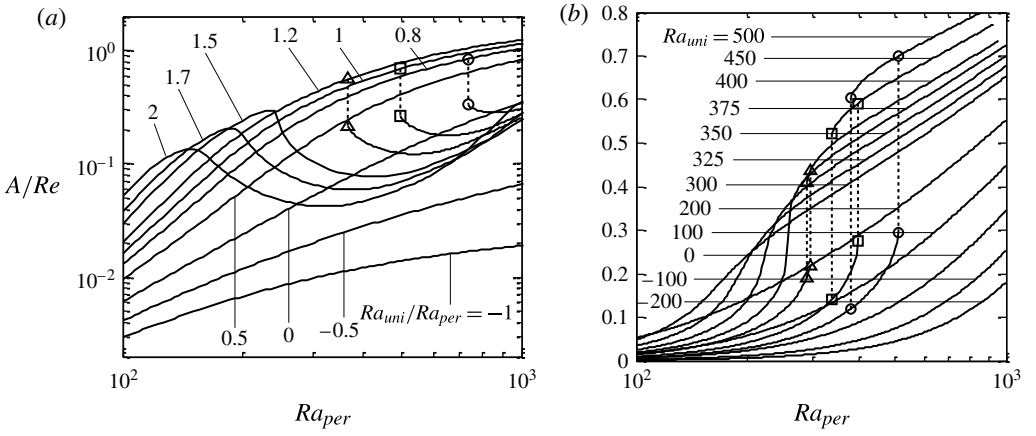

FIGURE 7. Variations of the pressure gradient correction A/Re as a function of Ra_{per} for $\alpha = 2$ and $Re = 1$ for different levels of the uniform heating measured in terms of either Ra_{uni}/Ra_{per} (a) or Ra_{uni} (b).

2 in figure 7(a). The most effective heating corresponds to $Ra_{uni}/Ra_{per} \approx 0.75$ as it does not trigger secondary states. The reader may note that the system performance with secondary states may still be better than that achieved using purely spatially modulated heating. In figure 7(b) the strength of the uniform heating is expressed in absolute form, i.e. in terms of Ra_{uni}, as this might be better suited for experimental planning. A single state exists for $Ra_{uni} < 400$ for all values of Ra_{per}. Within this range, the largest drag reduction is found for the largest values of Ra_{per}. A very rapid change occurs for $Ra_{per} \approx 400$, where a small change of Ra_{per} may result in a two- to threefold change of the pressure gradient correction. Stronger uniform heating ($Ra_{uni} \geqslant 400$) may lead to the formation of secondary states. The use of small Ra_{per} and large Ra_{uni} results in a large deterioration of the system performance (see the zone for $Ra_{per} < 300$ and $Ra_{uni} > 400$ in figure 7b). The use of much larger Ra_{per} ($Ra_{per} > 500$) combined with large Ra_{uni} eliminates secondary states and provides a very good system performance, e.g. Ra_{per} combined with $Ra_{uni} = 500$ almost triples the reduction of the pressure gradient achieved with $Ra_{uni} = 0$.

Figure 8 displays variations of A/Re as a function of Ra_{uni} for a fixed value of Ra_{per}. In figure 8(a) a relative measure of the intensity of uniform heating is used, i.e. Ra_{uni}/Ra_{per}. An initial improvement of the system performance due to an increase of Ra_{uni}/Ra_{per} is followed by its deterioration if Ra_{uni}/Ra_{per} becomes too large. Figure 9 illustrates changes in the flow topology due to an increase of Ra_{uni}/Ra_{per} from 0 (point A in figure 8a) to 0.5 (point B in figure 8a) with $Ra_{per} = 800$. An increase of the size of the separation bubbles is clearly visible and it correlates well with the increase of the intensity of motion from $\Psi_{max} = 3.6603$ to $\Psi_{max} = 6.8814$. Drag reduction similar to that achieved with $Ra_{per} = 800$ and no uniform heating ($Ra_{uni} = 0$) can also be achieved with $Ra_{uni}/Ra_{per} = 2.44$ (point C in figure 8a) and 3.92 (point E in figure 8a), and a better reduction can be achieved with $Ra_{uni}/Ra_{per} = 3.15$ (point D in figure 8a). Secondary states exist for such conditions, and the corresponding flow topologies are displayed in figure 10. There are two layers of separation bubbles alternating with zones of the in-flow trapped fluid, resulting in the appearance of several stream tubes channelling fluid from left to right. There is no qualitative change in the flow topologies from $Ra_{uni}/Ra_{per} = 2.44$ (figure 10a) to $Ra_{uni}/Ra_{per} = 3.15$ (figure 10b)

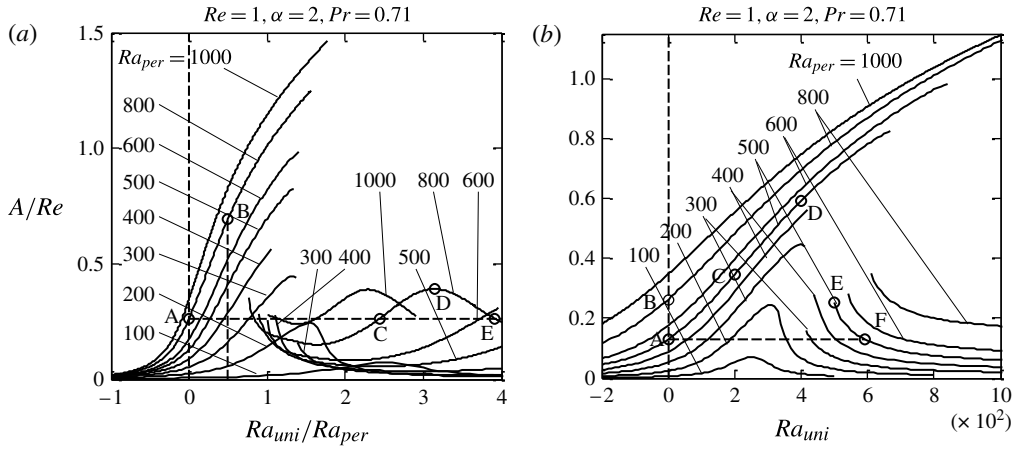

FIGURE 8. Variations of the pressure gradient correction A/Re as a function of either Ra_{uni}/Ra_{per} (a) or Ra_{uni} (b) for $\alpha = 2$ and $Re = 1$ for different values of Ra_{per}. Flow topologies for conditions corresponding to points A and B in (a) are displayed in figure 9, topologies corresponding to points C, D, E in (a) are displayed in figure 10, topologies corresponding to points A, C, D in (b) are displayed in figure 11 and topologies for points E, F in (b) are displayed in figure 12.

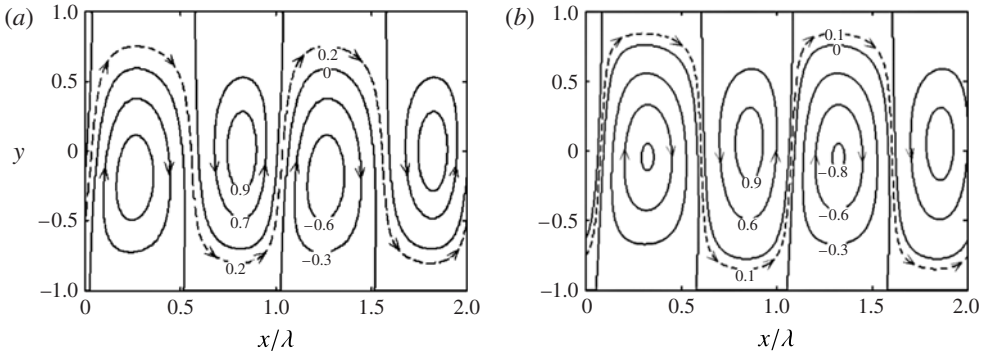

FIGURE 9. Flow topologies for $Re = 1$, $\alpha = 2$, $Ra_{per} = 800$ and $Ra_{uni}/Ra_{per} = 0$ (a, $\Psi_{max} = 3.6603$) and 0.5 (b, $\Psi_{max} = 6.8814$). The corresponding flow conditions correspond to points A and B in figure 8(a).

where three separate stream tubes exist, while only two stream tubes remain at $Ra_{uni}/Ra_{per} = 3.92$ (figure 10c). The delicate adjustment of the flow pattern results in the largest drag reduction for $Ra_{uni}/Ra_{per} = 3.15$ (figure 10b). It is remarkable that the same drag reduction can be achieved with the flow topology displayed in figure 9(a) as with the flow topologies shown in figure 10(a,c), while the topology displayed in figure 10(b) gives a better performance than the topology shown in figure 9(a).

Figure 8(b) displays variations of A/Re as a function of Ra_{uni}, and this offers an opportunity to discuss different strategies for an increase of A/Re in a potential experiment. Point A in this figure serves as a reference state where drag reduction of $A/Re = 0.13$ is achieved using purely spatially modulated heating with amplitude $Ra_{per} = 500$. The corresponding flow topology is displayed in figure 11(a) and the corresponding $\Psi_{max} = 2.6606$. Further reduction of drag can be achieved by increasing

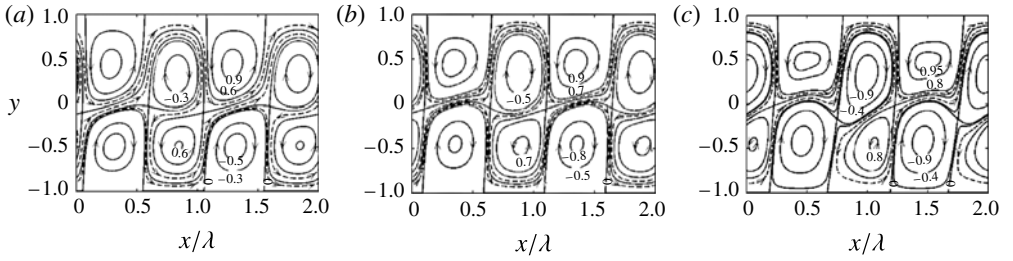

FIGURE 10. Flow topologies for $Re = 1$, $\alpha = 2$, $Ra_{per} = 800$ and $Ra_{uni}/Ra_{per} = 2.44$ (*a*, $\Psi_{max} = 3.0877$), 3.15 (*b*, $\Psi_{max} = 3.5442$) and 3.92 (*c*, $\Psi_{max} = 3.3575$). The corresponding flow conditions correspond to points C, D, E in figure 8(*a*).

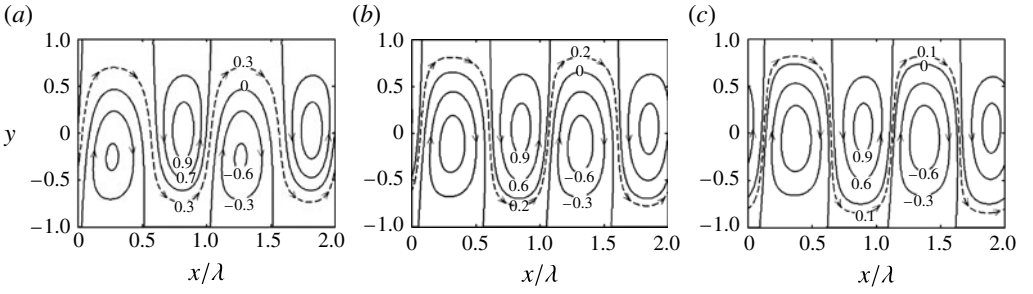

FIGURE 11. Flow topologies for $Re = 1$, $\alpha = 2$, $Ra_{per} = 500$ and $Ra_{uni} = 0$ (*a*, $\Psi_{max} = 2.6606$), 200 (*b*, $\Psi_{max} = 2.4244$) and 400 (*c*, $\Psi_{max} = 6.0279$). The corresponding flow conditions correspond to points A, C, D in figure 8(*b*).

Ra_{per} while keeping Ra_{uni} unchanged, e.g. point B in figure 8(*b*) which corresponds to $Ra_{per} = 800$ and results in $A/Re = 0.26$ and $\Psi_{max} = 3.6603$; the corresponding flow topology is displayed in figure 9(*a*). An alternative method for decreasing the drag involves increasing Ra_{uni} while keeping Ra_{per} fixed. Points C and D in figure 8(*b*) correspond to $Ra_{per} = 500$ and $Ra_{uni} = 200$, 400 respectively, and result in ($A/Re = 0.35$, $\Psi_{max} = 4.2444$) and ($A/Re = 0.59$, $\Psi_{max} = 6.0279$); the resulting flow topologies are displayed in figure 11(*b,c*). A further increase of Ra_{uni} leads to the formation of secondary states but drag lower than the reference drag can still be achieved. Point E in figure 8(*b*) illustrates such a situation where $Ra_{uni} = 500$ was used, resulting in $A/Re = 0.25$ and $\Psi_{max} = 3.5033$. The corresponding flow topology is displayed in figure 12(*a*). A further increase of Ra_{uni} complicates the flow structure and reduces the drag reduction. The drag reduction at $Ra_{uni} = 590$ (point F in figure 8*b*) is the same as for $Ra_{uni} = 0$ (point A in figure 8*b*), but the flow structure is very complex and involves two separate stream tubes, as shown in figure 12(*b*).

Figure 13 provides aggregate information about the dependence of A/Re on α and Ra_{per}. It can be seen that the highest drag reduction that can be achieved within the range of parameters studied is $A/Re \approx 0.3$ for $Ra_{uni} = 0$, $A/Re \approx 1$ for $Ra_{uni}/Ra_{per} = 0.5$ and $A/Re > 1$ for $Ra_{uni}/Ra_{per} = 1$, although one must remember about the avoidance of secondary states in the latter case. The most effective heating wavenumber changes from $\alpha \approx 1.8$ to $\alpha \approx 2.1$ when Ra_{per} varies from 100 to 1000 and $Ra_{uni} = 0$, it changes from $\alpha \approx 1.8$ to $\alpha \approx 2.5$ for $Ra_{uni}/Ra_{per} = 0.5$ and from $\alpha \approx 1.8$ to $\alpha \approx 3$ for $Ra_{uni}/Ra_{per} = 1$. Figure 14 provides aggregate information about the effects of Re.

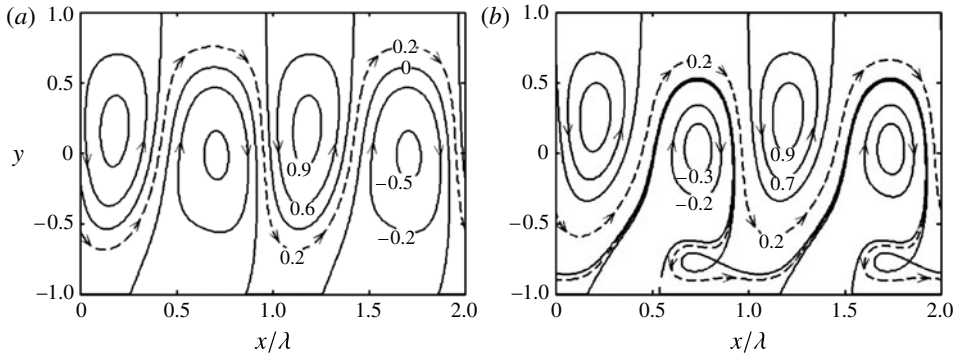

FIGURE 12. Flow topologies for $Re = 1$, $\alpha = 2$, $Ra_{per} = 500$ and $Ra_{uni} = 500$ (figure 12*a*, $\Psi_{max} = 3.5033$) and 590 (figure 12*b*, $\Psi_{max} = 2.6474$). The corresponding flow conditions correspond to points E, F in figure 8(*b*).

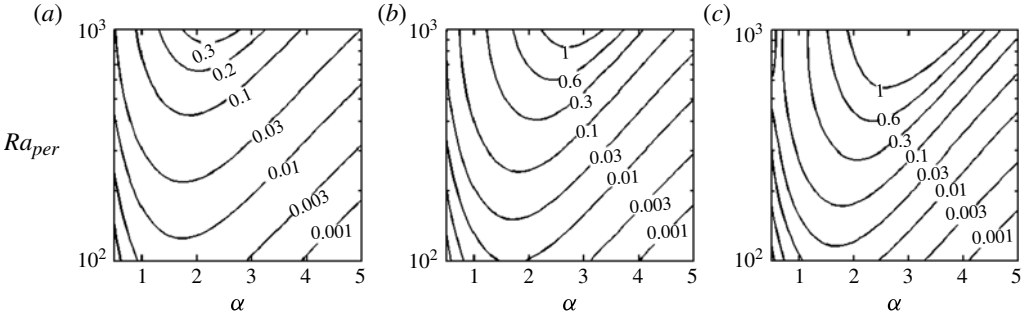

FIGURE 13. Variations of the pressure gradient correction A/Re as a function of α and Ra_{per} for the uniform heating corresponding to $Ra_{uni}/Ra_{per} = 0$, 0.5, 1 (*a–c* respectively) for $Re = 1$.

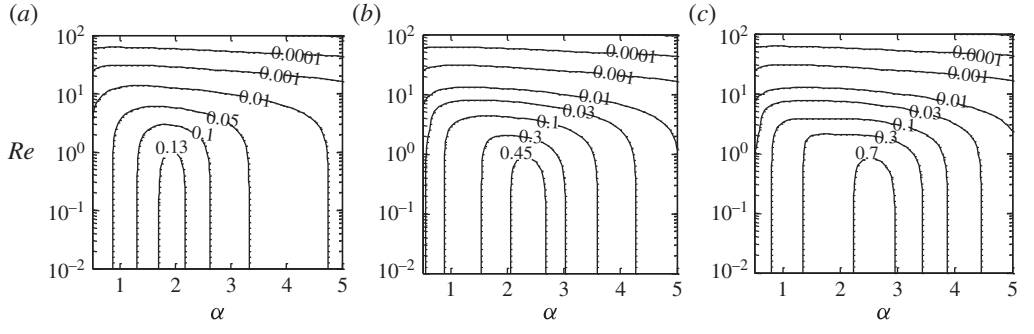

FIGURE 14. Variations of the pressure gradient correction A/Re as a function of α and Re for $Ra_{per} = 500$ and $Ra_{uni} = 0$, 0.5, 0.75 (*a–c* respectively).

A rapid decrease of the drag reduction occurs for $Re > 10$ regardless of the type of heating. As a matter of fact, $A/Re \approx 0.01$ for $Re = 10$ for all cases considered. The most effective heating wavenumber is not affected by an increase of uniform heating.

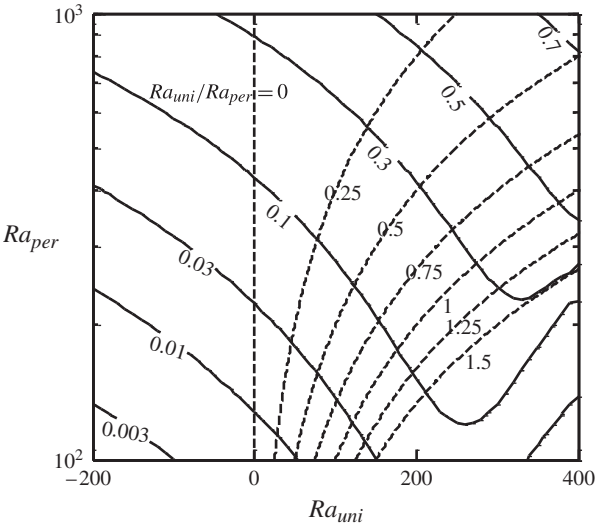

FIGURE 15. Variations of the pressure gradient correction A/Re as a function of Ra_{per} and Ra_{uni} for $\alpha = 2$ and $Re = 1$. Solid lines represent isolines of A/Re and dashed lines identify locations of $Ra_{per}/Re_{uni} = \text{const.}$ in the (Ra_{per}, Ra_{uni}) plane.

Figure 15 displays variations of A/Re as a function of Ra_{per} and Ra_{uni} and provides information about the best combination of both types of heating. It can be seen that the best system performance corresponds to the largest Ra_{per} and the largest Ra_{uni}. Secondary states are generated when Ra_{uni} is large but Ra_{per} is not sufficiently large (right bottom corner in figure 15); such conditions should be avoided as they result in deterioration of the system performance. The same figure provides information about the heating conditions at the lower wall. Local cooling is avoided when $Ra_{uni}/Ra_{per} > 0.5$ and this is very important in applications. Secondary flows can be avoided for $Ra_{uni}/Ra_{per} < 1$. The zone between these two limits is likely to be of the most importance in applications.

6.3. *Analysis of heat transfer*

The net heat transfer across the channel resulting from the applied heating is illustrated in figure 16, which displays variations of the average Nusselt number Nu_{av} based on the temperature scale T_{per} and defined as

$$Nu_{av} = \frac{1}{\lambda}\int_0^{\lambda}\left(\left.\frac{\mathrm{d}\theta_T}{\mathrm{d}y}\right|_{y=-1}\right)\mathrm{d}x = \frac{Ra_{uni}}{2Ra_{per}} - \left.\frac{\mathrm{d}\phi^{(0)}}{\mathrm{d}y}\right|_{y=-1}, \tag{6.17}$$

as a function of α and Ra_{per} for $Ra_{uni}/Ra_{per} = 0$, 0.5, 1 and for $Re = 1$, i.e. for the same conditions as used in figure 14 for illustration of variations of the pressure gradient reduction. This heat flow is driven mostly by conduction (compare figure 16*a* with figure 16*b*,*c*) and might be viewed as an energy loss. The largest heat flow occurs for $\alpha \approx 1$–1.5 while the largest pressure gradient reduction is found for $\alpha \approx 2$–2.5, and this suggests that a judicious selection of α can be used to reduce the energy cost.

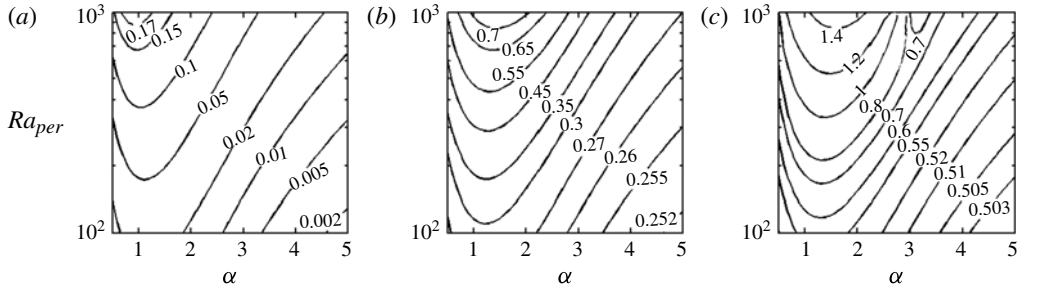

FIGURE 16. Variations of the average Nusselt number Nu_{av} as a function of α and Ra_{per} for $Ra_{uni}/Ra_{per} = 0,\ 0.5,\ 1$ (a–c respectively) for $Re = 1$.

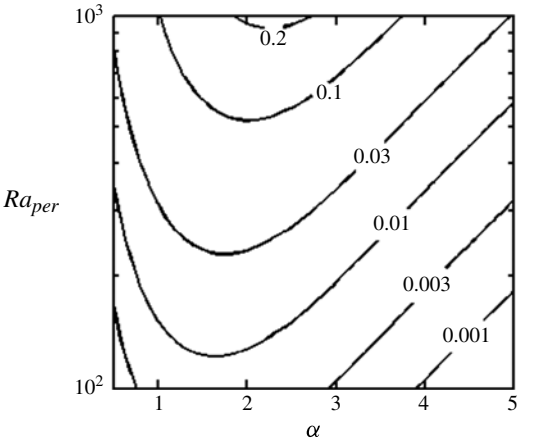

FIGURE 17. Variations of the pressure gradient correction A/Re for $Re = 1$ as a function of α and Ra_{per} for a channel with an insulated upper wall and subject to periodic heating at the lower wall.

The real role of transverse heat flow is, however, more complex. To illustrate this point, consider a channel with the upper wall insulated, which eliminates this heat flow. The formulation of the corresponding problem is given in appendix D and the resulting field equations have been solved using the same technique as described in § 3. The results presented in figure 17 demonstrate up to 50 % reduction of the pressure gradient correction when the isothermal upper wall is replaced with an insulated wall (compare figure 16*a* with figure 17). This suggests that a higher drag reduction is achieved when heating creates both large horizontal and large vertical temperature gradients; if one is interested in a high drag reduction, the energy costs associated with the creation of such gradients must be accepted. This point is well illustrated by comparing figure 17 with figure 14(*a*–*c*) in this particular order as it corresponds to progressively larger vertical temperature gradients combined with the same horizontal gradients.

Information about the horizontal heat flow is gained by looking at the heat flux leaving the lower wall per half heating wavelength. It is convenient to express this heat flux in terms of the Nusselt number Nu_h, defined as

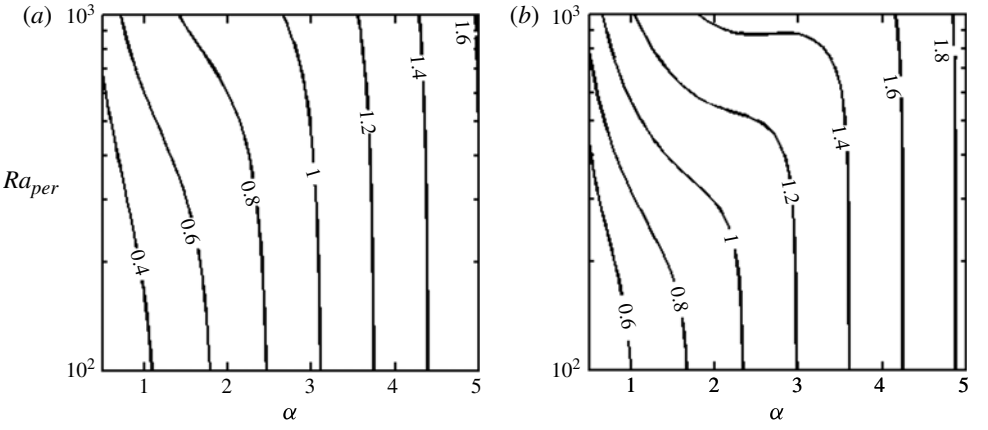

FIGURE 18. Variations of the Nusselt number for the half heating wavelength Nu_h (see (6.18)) as a function of α and Ra_{per} for $Ra_{uni}/Ra_{per} = 0$, 0.5 (*a*,*b* respectively) for $Re = 1$.

$$Nu_h = \frac{2}{\lambda} Pr \int_{-\lambda/4}^{\lambda/4} \left(\frac{\partial \theta_T}{\partial y} \right) \Big|_{y=-1} = \left\{ \frac{Ra_{uni}}{2Ra_{per}} \right\} + \left\{ \frac{\alpha}{2\pi} [\coth(\alpha) + \tanh(\alpha)] \right\} - \left\{ \frac{2}{\lambda} Pr \int_{-\lambda/4}^{\lambda/4} \left(\frac{\partial \theta_1}{\partial y} \Big|_{y=-1} \right) \mathrm{d}x \right\}, \tag{6.18}$$

where the first term on the right-hand side accounts for the conduction due to the uniform heating, the second one accounts for the conduction due to the periodic heating and the third one accounts for the convective effects. Figure 18 displays variations of Nu_h as a function of Ra_{per} and α, while figure 19 displays variations of the convective effects only, i.e. the third term in (6.18). It can be seen that the horizontal heat fluxes are much larger than the net heat flow across the channel (compare figure 18 with figure 16), with conductive effects providing the largest contribution (compare figure 18 with figure 19). It may be concluded that the main energy cost is associated with the creation of the horizontal temperature gradients.

The results presented in this paper suggest the use of spatially modulated heating as a method for intensification and/or optimization of the heat transfer, which is typically measured in terms of the ratio of the transverse heat flux and the pressure gradient required to maintain the flow (Fiebig 1995; Jacobi & Shah 1998; Ligrani, Oliviera & Blaskovich 2003). The heat flow in the case of uniform heating is driven under subcritical conditions by conduction only; one can increase its magnitude by using the supercritical conditions but at a cost of increased pressure loss (Gage & Reid 1968). The heat flow in the case of spatially modulated heating increases above its conductive base level and, at the same time, the pressure gradient decreases below the isothermal reference level. The gains are similar to those reported by Yamamoto, Hasegawa & Kasagi (2013), who achieved simultaneous drag reduction and heat transfer enhancement in turbulent flow using wall waves of suction/blowing travelling in the downstream direction. The present system is simpler due to its passive character.

The question of net gain, i.e. determination whether the reduction of the drag overcomes the costs of the heating, is difficult to answer. It has been shown that the overall viscous dissipation in an isothermal channel under a constant flow rate

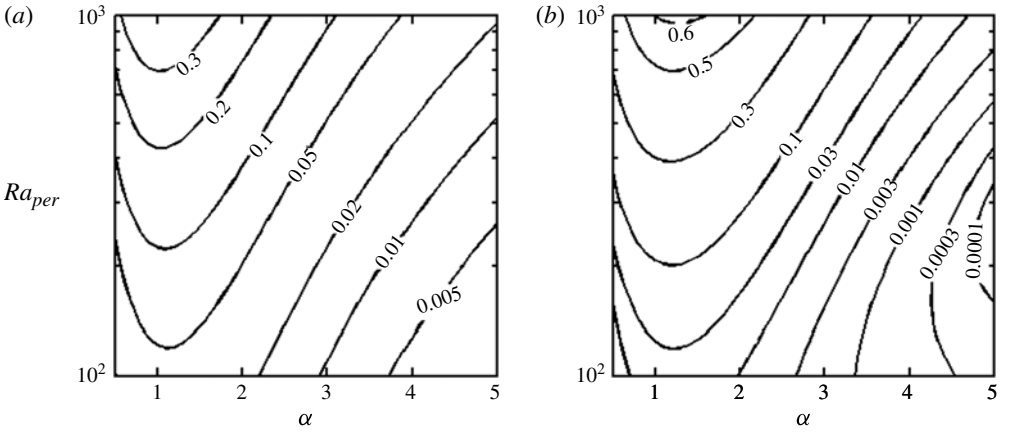

FIGURE 19. Variations of the convective component of the Nusselt number for the half heating wavelength Nu_h (see the third term on the right-hand side of (6.18)) as a function of α and Ra_{per} for $Ra_{uni}/Ra_{per} = 0,\ 0.5$ (a,b respectively) for $Re = 1$.

reaches a minimum for a laminar parabolic profile (Bewley 2009; Fukugata, Sugiyama & Kasagi 2009), and thus the overall energy consumption is always higher for controlled flow than for uncontrolled flow. This statement remains to be proven for a non-isothermal flow but probably remains valid. The cost of heating is a strong function of the heating technique but could be marginal if the heat supply were sufficiently inexpensive, e.g. waste heat. One can also look at the heating-induced drag reduction as an alternative pumping method where the total required pressure difference between the entrance and exit from the conduit is partially replaced by the heating-induced propulsive force distributed along the channel length. This pumping method may prove to be advantageous for long conduits and may provide an alternative to peristaltic pumping (Takagi & Balmforth 2011).

Our analysis has been carried out using the Boussinesq approximation and one needs to look at the limits of its applicability. The critical value of Ra_{uni} required to induce natural convection in the case of a uniformly heated lower wall and using the Boussinesq fluid model is $Ra_{uni,cr} = 213.5$; this value has been confirmed in numerous experiments (Gage & Reid 1968). The analysis described in this paper considered $Ra_{uni} < 1000$ and $Ra_{per} < 1000$, with the bulk of the results obtained for $Ra_{uni} < 400$, $Ra_{per} < 500$, where the Boussinesq approximation should be able to capture the basic mechanisms. The more extreme parameter values probably enter into the zone where real gas effects become important but are included in this presentation in order to illustrate the physical trends. It remains to be determined what role real gas effects play and under what conditions they need to be accounted for.

It is useful to return to dimensional quantities in order to assist with the interpretation of the results. The presented results have been obtained with $Pr = 0.71$ (air). We now assume atmospheric pressure and a reference temperature of $T_{ref} = 17$ °C to obtain a conductivity $k = 0.0263$ (W m^{-1} K^{-1}), specific heat $c = 1007$ (J kg^{-1} K^{-1}), thermal diffusivity $\kappa = k/\rho c = 22.5 \times 10^{-6}$ (m^2 s^{-1}), dynamic viscosity $\mu = 184.6 \times 10^{-7}$ (N s m^{-2}), kinematic viscosity $\nu = 15.89 \times 10^{-6}$ (m^2 s^{-1}), density $\rho = 1.1614$ (kg m^{-3}), thermal expansion coefficient $\Gamma = 1/(17 + 273) = 1/300$ (K^{-1}) and gravitational acceleration $g = 9.81$ (m s^{-2}) (Bergman *et al.* 2011). This leads to $Ra_{uni} = g\Gamma h^3 T_{uni}/\nu\kappa = 91.146 \times 10^6 h^3 T_{uni}$ and $Ra_{per} =$

$g\Gamma h^3 T_{per}/\nu\kappa = 91.146 \times 10^6 h^3 T_{per}$. If we assume a permissible temperature difference of $\Delta T = 10$ °C ($T_{uni} = T_{per} = 10$ °C) we obtain $Ra_{uni} = Ra_{per} = 914.6 \times 10^6 h^3$. Assuming $Ra_{uni} = Ra_{per} = 200$ leads to $h = 0.006$ (m). The same calculation for $Ra_{uni} = Ra_{per} = 500$ leads to $h = 0.0095$ (m). Doubling the permissible temperature difference to $\Delta T = 20$ °C leads to $h = 0.00479$ (m) for $Ra_{uni} = Ra_{per} = 200$ and $h = 0.0065$ (m) for $Ra_{uni} = Ra_{per} = 500$. The present results are, thus, applicable to channels with heights of a few millimetres. A proper account of real gas effects should provide means for expansion of the applicability of the results to a wider range of temperature differences.

7. Summary

The reduction of pressure losses in a pressure-driven flow in a heated channel has been analysed. Detailed quantitative results have been presented for the Prandtl number $Pr = 0.71$, which well approximates the properties of air. The heating has to have a spatially modulated component in order to reduce pressure losses. This heating generates a buoyancy field; this leads to the formation of separation bubbles which isolate the stream from direct contact with the bounding wall. The buoyancy force drives motion inside the bubbles; this generates a propulsive force which contributes to reduction of the pressure loss. The drag reducing effect can be magnified by increasing the vertical and horizontal temperature gradients as this would lead to a more intense convection. It has been demonstrated that use of a proper combination of spatially modulated heating and spatially uniform heating produces the desired effect and the drag reduction can be increased almost threefold (compared with the drag reduction achieved without uniform heating) within the range of parameters studied. The use of an excessively large uniform heating component leads to the formation of secondary states, and this causes a significant drop in the reduction of pressure losses. The use of large modulated heating together with large uniform heating avoids the creation of secondary states and provides the best opportunity for the reduction of pressure losses. Use of large uniform heating and small modulated heating should be avoided. The appearance of secondary states does not necessarily imply a deterioration of the system performance below that achieved using purely modulated heating; such a system may have pressure losses smaller than those achieved with purely modulated heating, and this offers opportunities for many applications. It has been shown that the drag reducing effect is negligible for heating with long-wavelength spatial modulations as well as with short-wavelength modulations. It has also been shown that the drag reducing effect rapidly decreases when the flow Reynolds number exceeds $Re = 10$, regardless of whether the uniform heating is used or not. The magnitude of drag reduction can reach up to 75 % of the isothermal value.

The reader may note that identification of the net energy effect and determination of whether or not it is favourable require a system-level study, which must include the costs of producing the desired wall temperature distribution as well as the required energy input.

There is a need for experimental verification of our predictions. The heating strategy analysed in this paper provides a basis for the design of an effective experiment as the results show that local cooling is not required; the desired effect can be achieved simply by using non-uniform heating along the lower wall.

Acknowledgements

This work has been carried out with support from the Natural Sciences and Engineering Research Council (NSERC) of Canada. The authors would like to thank Dr E. Savory for proofreading of the manuscript.

Appendix A

Definitions of functions used in § 4:

$$\hat{\hat{\theta}}_{00} = \frac{1}{4} - \frac{y}{4}, \tag{A 1}$$

$$\hat{\hat{\theta}}_{02} = -\frac{y^3}{24} + \frac{y^2}{8} + \frac{y}{24} - \frac{1}{8}, \tag{A 2}$$

$$\hat{\hat{\theta}}_{04} = -\frac{y^5}{480} + \frac{y^4}{96} + \frac{y^3}{144} - \frac{y^2}{16} - \frac{7y}{1440} + \frac{5}{96}, \tag{A 3}$$

$$F_{U1}(y) = \frac{y^4}{96} - \frac{y^3}{24} - \frac{y^2}{80} + \frac{y}{24} + \frac{1}{480}, \tag{A 4}$$

$$F_{V2}(y) = -\frac{y^5}{480} + \frac{y^4}{96} + \frac{y^3}{240} - \frac{y^2}{48} - \frac{y}{480} + \frac{1}{96}, \tag{A 5}$$

$$F_{P0}(y) = -\frac{y^2}{8} + \frac{y}{4} + \frac{1}{40}, \tag{A 6}$$

$$F_{\Theta 1} = -\frac{y^5}{80} + \frac{y^4}{48} + \frac{y^3}{24} - \frac{y^2}{8} - \frac{7y}{240} + \frac{5}{48}, \tag{A 7}$$

$$F_{U21}(y) = -\frac{y^8}{26\,880} + \frac{y^7}{10\,080} + \frac{y^6}{2880} - \frac{y^5}{480} - \frac{7y^4}{5760} + \frac{5y^3}{288} + \frac{107y^2}{100\,800} - \frac{31y}{2016} - \frac{1}{6400}, \tag{A 8}$$

$$F_{U22}(y) = -\frac{y^8}{8960} + \frac{y^7}{2016} + \frac{7y^6}{14\,400} - \frac{y^5}{480} - \frac{y^4}{1152} + \frac{y^3}{288} + \frac{19y^2}{33\,600} - \frac{19y}{10\,080} - \frac{29}{403\,200}, \tag{A 9}$$

$$F_{V31}(y) = -\frac{y^9}{241\,920} + \frac{y^8}{80\,640} + \frac{y^7}{20\,160} - \frac{y^6}{2880} - \frac{7y^5}{28\,800} + \frac{5y^4}{1152} + \frac{107y^3}{302\,400} - \frac{31y^2}{4032} - \frac{y}{6400} + \frac{33}{8960}, \tag{A 10}$$

$$F_{V32}(y) = -\frac{y^9}{80\,640} + \frac{y^8}{16\,128} + \frac{y^7}{14\,400} - \frac{y^6}{2880} - \frac{y^5}{5760} + \frac{y^4}{1152} + \frac{19y^3}{100\,800} - \frac{19y^2}{20\,160} - \frac{29y}{403\,200} + \frac{29}{80\,640}, \tag{A 11}$$

$$F_{P1} = -\frac{y^6}{480} + \frac{y^5}{240} + \frac{y^4}{96} - \frac{y^3}{24} - \frac{7y^2}{480} + \frac{5y}{48} + \frac{107}{50\,400}, \tag{A 12}$$

$$F_{\Theta 21} = \frac{y^7}{26\,880} - \frac{y^6}{3840} + \frac{y^5}{6400} + \frac{y^4}{1280} - \frac{y^3}{1280} - \frac{y^2}{1280} + \frac{79}{134\,400}y + \frac{1}{3840}, \tag{A 13}$$

$$F_{\Theta 22} = \frac{1}{201\,600}\left(5y^7 - 35y^6 - 21y^5 + 175y^4 + 35y^3 - 525y^2 - 19y + 385\right), \tag{A 14}$$

$$F_{\Theta 23} = \frac{1}{201\,600}\left(35y^9 - 75y^8 - 260y^7 + 980y^6 + 714y^5 - 3850y^4 - 980y^3 + 10\,500y^2 + 491y - 7555\right), \tag{A 15}$$

$$F_{\Theta 24} = -\frac{y^7}{40\,320} + \frac{y^6}{5760} - \frac{y^5}{4800} - \frac{y^4}{2880} + \frac{y^3}{1152} - \frac{y^2}{1920} - \frac{1}{1575}y + \frac{1}{1440}. \tag{A 16}$$

Appendix B

Definitions of functions used in § 5:

$$G_{U41}(\eta) = \tfrac{1}{192}(24\eta + 6\eta^2 + 2\eta^3 - \eta^4), \tag{B 1}$$
$$G_{U42}(\eta) = \tfrac{1}{192}(30\eta + 3\eta^2 - 2\eta^3 - \eta^4), \tag{B 2}$$
$$G_{V41}(\eta) = \tfrac{1}{192}(12\eta^2 + 6\eta^3 + 2\eta^4), \tag{B 3}$$
$$G_{V42}(\eta) = \tfrac{1}{192}(15\eta^2 + 6\eta^3 + \eta^4), \tag{B 4}$$
$$G_{P31}(\eta) = \tfrac{1}{96}(18 + 6\eta + 6\eta^2 + 4\eta^3), \tag{B 5}$$
$$G_{P32}(\eta) = \tfrac{1}{96}(27 + 12\eta - 4\eta^2), \tag{B 6}$$
$$G_{\Theta 41}(\eta) = \tfrac{1}{384}(3\eta + 3\eta^2 + 2\eta^3), \tag{B 7}$$
$$G_{\Theta 42}(\eta) = \tfrac{1}{48}(15 + 15\eta + 10\eta^2 + 3\eta^3), \tag{B 8}$$
$$G_{U51}(\eta) = -360\eta - 90\eta^2 - 30\eta^3 + 6\eta^5, \tag{B 9}$$
$$G_{U52}(\eta) = -270\eta - 45\eta^2 + 5\eta^4 + 2\eta^5, \tag{B 10}$$
$$G_{U53}(\eta) = 3\eta - 3\eta^2 - 8\eta^3 + 4\eta^4, \tag{B 11}$$
$$G_{U54}(\eta) = -15\eta - 3\eta^2 + 4\eta^3 + 4\eta^4, \tag{B 12}$$
$$G_{V51}(\eta) = 180\eta^2 + 90\eta^3 + 30\eta^4 + 6\eta^5, \tag{B 13}$$
$$G_{V52}(\eta) = 135\eta^2 + 60\eta^3 + 15\eta^4 + 2\eta^5, \tag{B 14}$$
$$G_{V53}(\eta) = -3\eta^2 + 4\eta^4, \tag{B 15}$$
$$G_{V54}(\eta) = 15\eta^2 + 12\eta^3 + 4\eta^4, \tag{B 16}$$
$$G_{P41}(\eta) = -54 - 18\eta - 18\eta^2 - 12\eta^3 - 6\eta^4, \tag{B 17}$$
$$G_{P42}(\eta) = -45 - 18\eta - 6\eta^2 + 2\eta^4, \tag{B 18}$$
$$G_{P43}(\eta) = 45 + 180\eta + 360\eta^2 + 480\eta^3 - 1440\eta^4 + 384\eta^5, \tag{B 19}$$
$$G_{P44}(\eta) = 20(-27 - 24\eta + 32\eta^3), \tag{B 20}$$
$$G_{\Theta 51}(\eta) = 27\eta + 27\eta^2 + 18\eta^3 + 8\eta^4 + 2\eta^5, \tag{B 21}$$
$$G_{\Theta 52}(\eta) = 36\eta + 72\eta^2 + 32\eta^3 + 8\eta^4, \tag{B 22}$$
$$G_{\Theta 53}(\eta) = 51\eta + 102\eta^2 + 56\eta^3 + 16\eta^4, \tag{B 23}$$
$$G_{U61}(\eta) = 3(-270\eta - 45\eta^2 + 5\eta^4 + 2\eta^5), \tag{B 24}$$
$$G_{U62}(\eta) = 16(-2250\eta - 720\eta^2 - 345\eta^3 - 452\eta^4 + 9\eta^5 + 8\eta^6), \tag{B 25}$$
$$G_{U63}(\eta) = 48(-900\eta - 180\eta^2 - 30\eta^3 + 5\eta^4 + 5\eta^5 + \eta^6), \tag{B 26}$$
$$G_{U64}(\eta) = 16(-2070\eta - 630\eta^2 - 285\eta^3 + 18\eta^5 + 4\eta^6), \tag{B 27}$$
$$G_{V61}(\eta) = -3(135\eta^2 + 60\eta^3 + 15\eta^4 + 2\eta^5), \tag{B 28}$$
$$G_{V62}(\eta) = 16(1125\eta^2 + 615\eta^3 + 240\eta^4 + 57\eta^5 + 8\eta^6), \tag{B 29}$$
$$G_{V63}(\eta) = 48(450\eta^2 + 210\eta^3 + 60\eta^4 + 11\eta^5 + \eta^6), \tag{B 30}$$
$$G_{V64}(\eta) = 16(1035\eta^2 + 555\eta^3 + 210\eta^4 + 42\eta^5 + 4\eta^6), \tag{B 31}$$
$$G_{P51}(\eta) = 5(45 + 18\eta + 6\eta^2 - 2\eta^4), \tag{B 32}$$

$$G_{P52}(\eta) = 16(-510 - 135\eta - 135\eta^2 - 90\eta^3 - 25\eta^4 - 4\eta^5), \tag{B 33}$$

$$G_{P53}(\eta) = 16(480 + 135\eta + 135\eta^2 + 90\eta^3 + 20\eta^4 + 2\eta^5), \tag{B 34}$$

$$G_{P54}(\eta) = 32(-360 - 135\eta - 60\eta^2 - 15\eta^3 + 5\eta^4 + 3\eta^5), \tag{B 35}$$

$$G_{\Theta 61}(\eta) = \tfrac{1}{3\,145\,728}(-18 - 36\eta - 36\eta^2 - 32\eta^3 - 16\eta^4), \tag{B 36}$$

$$G_{\Theta 62}(\eta) = \tfrac{1}{3\,145\,728}(843 + 1584\eta + 1380\eta^2 + 688\eta^3 + 176\eta^4), \tag{B 37}$$

$$G_{\Theta 63}(\eta) = 245\,760(3\eta + 3\eta^2 + 2\eta^3), \tag{B 38}$$

$$G_{\Theta 64}(\eta) = 16\,384(855\eta + 855\eta^2 + 570\eta^3 + 285\eta^4 + 96\eta^5 + 20\eta^6), \tag{B 39}$$

$$G_{\Theta 65}(\eta) = \tfrac{1}{21\,233\,664}(-5\eta - 15\eta^2 + 24\eta^3 + 36\eta^4), \tag{B 40}$$

$$G_{\Theta 66}(\eta) = \tfrac{1}{21\,233\,664}(127\eta + 381\eta^2 + 482\eta^3 + 252\eta^4), \tag{B 41}$$

$$G_{\Theta 67}(\eta) = -\tfrac{1}{7680}(7200\eta + 7200\eta^2 + 4800\eta^3 + 2000\eta^4 + 560\eta^5 + 80\eta^6), \tag{B 42}$$

$$G_{\Theta 68}(\eta) = \tfrac{1}{7680}(135\eta + 135\eta^2 + 90\eta^3 + 25\eta^4), \tag{B 43}$$

$$G_{\Theta 69}(\eta) = \tfrac{1}{7680}(270\eta + 270\eta^2 + 180\eta^3 + 55\eta^4 + 10\eta^5), \tag{B 44}$$

$$G_{\Theta 70}(\eta) = \tfrac{1}{491\,520}(2205\eta + 4410\eta^2 + 2040\eta^3 + 600\eta^4 + 96\eta^5), \tag{B 45}$$

$$G_{\Theta 71}(\eta) = \tfrac{1}{49\,152}(171\eta + 342\eta^2 + 168\eta^3 + 56\eta^4 + 16\eta^5), \tag{B 46}$$

$$G_{X71}(\eta) = \tfrac{1}{3072}(-12\eta^3 - 4\eta^4 + 4\eta^5), \tag{B 47}$$

$$G_{X72}(\eta) = \tfrac{1}{3072}(-12\eta^3 + 4\eta^4 + 2\eta^5), \tag{B 48}$$

$$G_{X73}(\eta) = \tfrac{1}{480}(-90\eta^2 + 15\eta^4 + 8\eta^5 + 8\eta^6), \tag{B 49}$$

$$G_{X74}(\eta) = \tfrac{1}{960}(-135\eta^2 + 15\eta^3 + 60\eta^4 + 27\eta^5 + 7\eta^6), \tag{B 50}$$

$$G_{X75}(\eta) = \tfrac{1}{24\,576}(-189\eta^2 - 102\eta^3 - 28\eta^4 + 8\eta^5), \tag{B 51}$$

$$G_{X76}(\eta) = \tfrac{1}{24\,576}(-255\eta^2 - 90\eta^3 + 4\eta^4 + 8\eta^5), \tag{B 52}$$

$$G_{X81}(\eta) = \tfrac{1}{10\,240}(-60\eta^2 - 20\eta^3 + 2\eta^4 + 6\eta^5) \tag{B 53}$$

$$G_{X82}(\eta) = \tfrac{1}{10\,240}(-40\eta^2 - 5\eta^3 + 4\eta^4 + 2\eta^5) \tag{B 54}$$

$$G_{X83}(\eta) = \tfrac{1}{15\,360}(-135\eta^2 + 15\eta^3 + 15\eta^4 + 7\eta^5 + 2\eta^6) \tag{B 55}$$

$$G_{X84}(\eta) = \tfrac{1}{2880}(-1125\eta^2 - 105\eta^3 - 105\eta^4 + 12\eta^5 + 17\eta^6 + 8\eta^7) \tag{B 56}$$

$$G_{X85}(\eta) = \tfrac{1}{2880}(-1035\eta^2 - 75\eta^3 - 75\eta^4 + 42\eta^5 + 22\eta^6 + 4\eta^7) \tag{B 57}$$

$$G_{X86}(\eta) = \tfrac{1}{2880}(-1350\eta^2 + 90\eta^3 + 90\eta^4 + 48\eta^5 + 18\eta^6 + 3\eta^7) \tag{B 58}$$

$$G_{X87}(\eta) = \tfrac{1}{122\,880}(1440\eta^2 + 720\eta^3 + 135\eta^4 - 4\eta^5 - 20\eta^6) \tag{B 59}$$

$$G_{X88}(\eta) = \tfrac{1}{122\,880}(1080\eta^2 + 480\eta^3 + 15\eta^4 - 48\eta^5 - 20\eta^6) \tag{B 60}$$

$$G_{X89}(\eta) = \tfrac{1}{1\,572\,864}(3\eta^2 - 9\eta^3 - 26\eta^4 + 32\eta^5 - 8\eta^6) \tag{B 61}$$

$$G_{X90}(\eta) = \tfrac{1}{1\,572\,864}(-15\eta^2 - 3\eta^3 + 4\eta^4 + 8\eta^5 - 8\eta^6) \tag{B 62}$$

$$G_{X91}(\eta) = \tfrac{1}{1920}(90\eta^4 + 30\eta^5 + 12\eta^6 + 6\eta^7) \tag{B 63}$$

$$G_{X92}(\eta) = \tfrac{1}{1920}(75\eta^4 + 30\eta^5 + 9\eta^6 + 2\eta^7) \tag{B 64}$$

$$G_{X93}(\eta) = \tfrac{1}{1\,572\,864}(-9\eta^2 + 3\eta^3 + 16\eta^4) \tag{B 65}$$

$$G_{X94}(\eta) = \tfrac{1}{1\,572\,864}(45\eta^2 + 33\eta^3 + 10\eta^4) \tag{B 66}$$

$$G_{U71}(\eta) = \tfrac{1}{3072}(12\eta + 12\eta^2 + 8\eta^3 + 4\eta^4 + \eta^5), \tag{B 67}$$

$$G_{U72}(\eta) = \tfrac{1}{24\,576}(66\eta + 66\eta^2 + 44\eta^3 + 22\eta^4 + 4\eta^5), \tag{B 68}$$

$$G_{U81}(\eta) = \tfrac{1}{81\,920}(375 + 750\eta + 750\eta^2 + 500\eta^3 + 250\eta^4 + 76\eta^5 + 12\eta^6), \quad \text{(B 69)}$$

$$G_{U82}(\eta) = \tfrac{1}{20\,480}(45 + 90\eta + 90\eta^2 + 60\eta^3 + 30\eta^4 + 8\eta^5 + \eta^6). \quad \text{(B 70)}$$

Appendix C. Weak uniform heating

Consider a situation where the convection is weak and, in addition, the uniform heating component is small, i.e. $\hat{\varepsilon} = |Ra_{uni}|Ra_{per} \ll 1$. The reference case of weak convection described in § 6.2.1 forms a starting point. When $\hat{\varepsilon} \ll 1$, solution (6.5) is assumed to be in the form

$$\begin{aligned}(u_1, v_1, p_1, \theta_1) \;=\; & \varepsilon\,[U_{10} + \hat{\varepsilon}U_{11} + 0(\hat{\varepsilon}^2),\, V_{10} + \hat{\varepsilon}V_{11} + 0(\hat{\varepsilon}^2),\, P_{10} + \hat{\varepsilon}P_{11} + 0(\hat{\varepsilon}^2),\\ & \Theta_{10} + \hat{\varepsilon}\Theta_{11} + 0(\hat{\varepsilon}^2)] + \varepsilon^2\,[U_{20} + \hat{\varepsilon}U_{21} + 0(\hat{\varepsilon}^2),\, V_{20} + \hat{\varepsilon}V_{21} + 0(\hat{\varepsilon}^2),\\ & P_{20} + \hat{\varepsilon}P_{21} + 0(\hat{\varepsilon}^2),\, \Theta_{20} + \hat{\varepsilon}\Theta_{21} + 0(\hat{\varepsilon}^2)] + 0(\varepsilon^3). \quad \text{(C 1)}\end{aligned}$$

Substitution of (C 1) into (2.6) and collection of terms proportional to ε result in the following two systems.

$$\text{System } 0(\varepsilon)\text{:}\quad \nabla^2 U_{10} - Reu_0\frac{\partial U_{10}}{\partial x} - ReV_{10}\frac{\mathrm{d}u_0}{\mathrm{d}y} - \frac{\partial P_{10}}{\partial x} = 0, \quad \text{(C 2}a\text{)}$$

$$\nabla^2 V_{10} - Reu_0\frac{\partial V_{10}}{\partial x} - \frac{\partial P_{10}}{\partial y} + Ra_{per}\Theta_{10} = -Ra_{per}Pr^{-1}\tilde{\theta}_0, \quad \text{(C 2}b\text{)}$$

$$\nabla^2\Theta_{10} - PrReu_0\frac{\partial \Theta_{10}}{\partial x} = Reu_0\frac{\partial\tilde{\theta}_0}{\partial x}, \quad \text{(C 2}c\text{)}$$

$$\frac{\partial U_{10}}{\partial x} + \frac{\partial V_{10}}{\partial y} = 0. \quad \text{(C 2}d\text{)}$$

$$\text{System } 0(\varepsilon\hat{\varepsilon})\text{:}\quad \nabla^2 U_{11} - Reu_0\frac{\partial U_{11}}{\partial x} - ReV_{11}\frac{\mathrm{d}u_0}{\mathrm{d}y} - \frac{\partial P_{11}}{\partial x} = 0, \quad \text{(C 3}a\text{)}$$

$$\nabla^2 V_{11} - Reu_0\frac{\partial V_{11}}{\partial x} - \frac{\partial P_{11}}{\partial y} + Ra_{per}\Theta_{11} = 0, \quad \text{(C 3}b\text{)}$$

$$\nabla^2\Theta_{11} - PrReu_0\frac{\partial \Theta_{11}}{\partial x} = -\frac{Ra_{uni}}{2|Ra_{uni}|}V_{10}, \quad \text{(C 3}c\text{)}$$

$$\frac{\partial U_{11}}{\partial x} + \frac{\partial V_{11}}{\partial y} = 0. \quad \text{(C 3}d\text{)}$$

The above systems can be rearranged into forms suitable for computations by introducing the following quantities: $\dddot{U}_{10} = \varepsilon U_{10}$, $\dddot{V}_{10} = \varepsilon V_{10}$, $\dddot{P}_{10} = \varepsilon P_{10}$, $\dddot{\Theta}_{10} = \varepsilon\Theta_{10}$, $\dddot{U}_{11} = \varepsilon U_{11}$, $\dddot{V}_{11} = \varepsilon V_{11}$, $\dddot{P}_{11} = \varepsilon P_{11}$, $\dddot{\Theta}_{11} = \varepsilon\Theta_{11}$, and noting that $\tilde{\theta}_0 = \hat{\tilde{\theta}}_0/\varepsilon = 0(1)$. The forcing on the right-hand side determines the form of the solution, i.e.

$$\begin{aligned}&[\dddot{U}_{10}(x,y), \dddot{V}_{10}(x,y), \dddot{P}_{10}(x,y), \dddot{\Theta}_{10}(x,y)]\\ &\quad = [\dddot{U}^{(1)}_{10}(y), \dddot{V}^{(1)}_{10}(y), \dddot{P}^{(1)}_{10}(y), \dddot{\Theta}^{(1)}_{10}(y)]\mathrm{e}^{\mathrm{i}\alpha x} + \text{c.c.}, \quad \text{(C 4}a\text{)}\\ &[\dddot{U}_{11}(x,y), \dddot{V}_{11}(x,y), \dddot{P}_{11}(x,y), \dddot{\Theta}_{11}(x,y)]\\ &\quad = [\dddot{U}^{(1)}_{11}(y), \dddot{V}^{(1)}_{11}(y), \dddot{P}^{(1)}_{11}(y), \dddot{\Theta}^{(1)}_{11}(y)]\mathrm{e}^{\mathrm{i}\alpha x} + \text{c.c.} \quad \text{(C 4}b\text{)}\end{aligned}$$

It can be shown that the solution retains the same form up to any order of $\hat{\varepsilon}$, i.e. it involves only a single Fourier component and does not generate any pressure gradient

correction. Substitution of (C 4) into (C 2) and (C 3) results in equations for the modal functions; these equations are not presented as they can be readily derived.

The pressure gradient correction is determined by systems $0(\varepsilon^2)$. The two leading-order systems have the following forms.

$$\text{System } 0(\varepsilon^2)\colon \nabla^2 U_{20} - Reu_0\frac{\partial U_{20}}{\partial x} - ReV_{20}\frac{\mathrm{d}u_0}{\mathrm{d}y} - \frac{\partial P_{20}}{\partial x} = U_{10}\frac{\partial U_{10}}{\partial x} + V_{10}\frac{\partial U_{10}}{\partial y}, \tag{C 5a}$$

$$\nabla^2 V_{20} - Reu_0\frac{\partial V_{20}}{\partial x} - \frac{\partial P_{20}}{\partial y} + Ra_{per}\Theta_{20} = U_{10}\frac{\partial V_{10}}{\partial x} + V_{10}\frac{\partial V_{10}}{\partial y}, \tag{C 5b}$$

$$\nabla^2\Theta_{20} - PrReu_0\frac{\partial \Theta_{20}}{\nabla x} = U_{10}\frac{\partial\tilde{\theta}_0}{\partial x} + V_{10}\frac{\partial\tilde{\theta}_0}{\partial y} + PrU_{10}\frac{\partial\Theta_{10}}{\partial x} + PrV_{10}\frac{\partial\Theta_{10}}{\partial y}, \tag{C 5c}$$

$$\frac{\partial U_{20}}{\partial x} + \frac{\partial V_{20}}{\partial y} = 0. \tag{C 5d}$$

$$\begin{aligned}\text{System } 0(\varepsilon^2\hat{\varepsilon})\colon &\nabla^2 U_{21} - Reu_0\frac{\partial U_{21}}{\partial x} - ReV_{21}\frac{\mathrm{d}u_0}{\mathrm{d}y} - \frac{\partial P_{21}}{\partial x}\\ &= U_{10}\frac{\partial U_{11}}{\partial x} + V_{10}\frac{\partial U_{11}}{\partial y} + U_{11}\frac{\partial U_{10}}{\partial x} + V_{11}\frac{\partial U_{10}}{\partial y},\end{aligned} \tag{C 6a}$$

$$\begin{aligned}&\nabla^2 V_{21} - Reu_0\frac{\partial V_{21}}{\partial x} - \frac{\partial P_{21}}{\partial y} + Ra_{per}\Theta_{21}\\ &= U_{10}\frac{\partial V_{11}}{\partial x} + V_{10}\frac{\partial V_{11}}{\partial y} + U_{11}\frac{\partial V_{10}}{\partial x} + V_{11}\frac{\partial V_{10}}{\partial y},\end{aligned} \tag{C 6b}$$

$$\begin{aligned}\nabla^2\Theta_{21} - PrReu_0\frac{\partial\Theta_{21}}{\partial x} = &-\frac{Ra_{uni}}{2|Ra_{uni}|}V_{20} + U_{11}\frac{\partial\tilde{\theta}_0}{\partial x} + V_{11}\frac{\partial\tilde{\theta}_0}{\partial y}\\ &+ PrU_{11}\frac{\partial\Theta_{10}}{\partial x} + PrV_{10}\frac{\partial\Theta_{11}}{\partial y} + PrU_{10}\frac{\partial\Theta_{11}}{\partial x} + PrV_{11}\frac{\partial\Theta_{10}}{\partial y},\end{aligned} \tag{C 6c}$$

$$\frac{\partial U_{21}}{\partial x} + \frac{\partial V_{21}}{\partial y} = 0. \tag{C 6d}$$

The solution of (C 5) has the form

$$[U_{20}(x,y), V_{20}(x,y), \Theta_{20}(x,y)] = \sum_{n=-2,0,2}[U_{20}^{(n)}(y), V_{20}^{(n)}(y), \Theta_{20}^{(n)}(y)]\mathrm{e}^{\mathrm{i}n\alpha x}, \tag{C 7a}$$

$$P_{20}(x,y) = \sum_{n=-2,0,2}P_{20}^{(n)}(y)\mathrm{e}^{\mathrm{i}n\alpha x} + A_{20}x. \tag{C 7b}$$

Substitution of (C 7) into (C 5), extraction of mode 0 from (C 5*a*) and solution of the resulting problem give

$$\varepsilon\dddot{U}_{20}^{(0)} = -\frac{1}{2}\varepsilon\dddot{A}_{20}(1-y^2) - \frac{1}{2}\int_{-1}^{1}\ddot{g}_{20}(y)\mathrm{d}y(1+y) + \int_{-1}^{y}\ddot{g}_{20}(\eta)\mathrm{d}\eta, \tag{C 8a}$$

$$\ddot{g}_{20}(y) = \ddot{V}_{10}^{(-1)}U_{10}^{(1)} + \ddot{V}_{10}^{(1)}\ddot{U}_{10}^{(-1)}, \tag{C 8b}$$

$$\varepsilon\dddot{A}_{20} = -\frac{3}{2}\int_{-1}^{1}\ddot{g}_{20}(y)\mathrm{d}y + \frac{3}{2}\int_{-1}^{1}\int_{-1}^{y}\ddot{g}_{20}(\eta)\mathrm{d}\eta\mathrm{d}y, \tag{C 8c}$$

$$\varepsilon^2 \left.\frac{\partial P_{20}}{\partial x}\right|_{mean} = \varepsilon^2 A_{20} = \varepsilon \dddot{A}_{20} = -\frac{3}{2}\int_{-1}^{1} \ddot{g}_{20}(y)\mathrm{d}y + \frac{3}{2}\int_{-1}^{1}\int_{-1}^{y} \ddot{g}_{20}(\eta)\mathrm{d}\eta\mathrm{d}y, \quad (\mathrm{C}\,8d)$$

where $\ddot{U}_{20}^{(0)} = \varepsilon U_{20}^{(0)}$, $\ddot{V}_{10}^{(1)} = \varepsilon V_{10}^{(1)}$, $\ddot{V}_{10}^{(-1)} = \varepsilon V_{10}^{(-1)}$, $\ddot{U}_{10}^{(1)} = \varepsilon U_{10}^{(1)}$, $\ddot{U}_{10}^{(-1)} = \varepsilon U_{10}^{(-1)}$, $\dddot{A}_{20} = \varepsilon A_{20}$. Equation (C 8*c*) gives the pressure gradient correction in the absence of uniform heating. The effect of uniform heating is captured by the solution of (C 6). Its functional form can be expressed as

$$[U_{21}(x,y), V_{21}(x,y), \Theta_{21}(x,y)] = \sum_{n=-2}^{2} [U_{21}^{(n)}(y), V_{21}^{(n)}(y), \Theta_{21}^{(n)}(y)]\mathrm{e}^{\mathrm{i}n\alpha x}, \quad (\mathrm{C}\,9a)$$

$$P_{21}(x,y) = \sum_{n=-2}^{2} P_{21}^{(n)}(y)\mathrm{e}^{\mathrm{i}n\alpha x} + A_{21}x. \quad (\mathrm{C}\,9b)$$

Substitution of (C 9) into (C 8), extraction of mode 0 from (C 6*a*) and solution of the resulting system give

$$\varepsilon \ddot{U}_{21}^{(0)} = -\frac{1}{2}\varepsilon \dddot{A}_{21}(1-y^2) - \frac{1}{2}\int_{-1}^{1} \ddot{g}_{21}(y)\mathrm{d}y(1+y) + \int_{-1}^{y} \ddot{g}_{21}(\eta)\mathrm{d}\eta, \quad (\mathrm{C}\,10a)$$

$$\ddot{g}_{21}(y) = \ddot{V}_{10}^{(-1)}\ddot{U}_{11}^{(1)} + \ddot{V}_{10}^{(1)}\ddot{U}_{11}^{(-1)} + \ddot{V}_{11}^{(-1)}\ddot{U}_{10}^{(1)} + \ddot{V}_{11}^{(1)}\ddot{U}_{10}^{(-1)}, \quad (\mathrm{C}\,10b)$$

$$\varepsilon \dddot{A}_{21} = -\frac{3}{2}\int_{-1}^{1} \ddot{g}_{21}(y)\mathrm{d}y + \frac{3}{2}\int_{-1}^{1}\int_{-1}^{y} \ddot{g}_{21}(\eta)\mathrm{d}\eta\mathrm{d}y, \quad (\mathrm{C}\,10c)$$

$$\begin{aligned}\varepsilon^2\hat{\varepsilon}\left.\frac{\partial P_{21}}{\partial x}\right|_{mean} &= \varepsilon^2\hat{\varepsilon}A_{21} = \varepsilon\hat{\varepsilon}\dddot{A}_{21} \\ &= \hat{\varepsilon}\left(-\frac{3}{2}\int_{-1}^{1} \ddot{g}_{21}(y)\mathrm{d}y + \frac{3}{2}\int_{-1}^{1}\int_{-1}^{y} \ddot{g}_{21}(\eta)\mathrm{d}\eta\mathrm{d}y\right), \end{aligned} \quad (\mathrm{C}\,10d)$$

where $\ddot{U}_{21}^{(0)} = \varepsilon U_{21}^{(0)}$, $\ddot{V}_{11}^{(1)} = \varepsilon V_{11}^{(1)}$, $\ddot{V}_{11}^{(-1)} = \varepsilon V_{11}^{(-1)}$, $\ddot{U}_{11}^{(1)} = \varepsilon U_{11}^{(1)}$, $\ddot{U}_{11}^{(-1)} = \varepsilon U_{11}^{(-1)}$, $\ddot{A}_{21} = \varepsilon A_{21}$. The total pressure gradient correction can now be expressed as

$$\begin{aligned}\left.\frac{\partial p_1}{\partial x}\right|_{mean} &= \varepsilon^2\left(\frac{\partial P_{20}}{\partial x} + \hat{\varepsilon}\frac{\partial P_{21}}{\partial x}\right)\Bigg|_{mean} = \varepsilon^2(A_{20} + \hat{\varepsilon}A_{21}) = \varepsilon(\dddot{A}_{20} + \hat{\varepsilon}A_{21}) \\ &= -\frac{3}{2}\int_{-1}^{1} \ddot{g}_{20}(y)\mathrm{d}y + \frac{3}{2}\int_{-1}^{1}\int_{-1}^{y} \ddot{g}_{20}(\eta)\mathrm{d}\eta\mathrm{d}y \\ &\quad + \hat{\varepsilon}\left(-\frac{3}{2}\int_{-1}^{1} \ddot{g}_{21}(y)\mathrm{d}y + \frac{3}{2}\int_{-1}^{1}\int_{-1}^{y} \ddot{g}_{21}(\eta)\mathrm{d}\eta\mathrm{d}y\right). \end{aligned} \quad (\mathrm{C}\,11)$$

The above relation demonstrates the linear dependence of the pressure gradient correction on the magnitude of the uniform heating for weak convection and small departures from purely periodic heating.

Appendix D. Channel with the upper wall insulated

Consider the flow in a channel described in § 2 but with the upper wall insulated. The same scaling as used in § 2 results in the conductive temperature field of the

form

$$\theta_0(x,y) = \hat{\hat{\theta}}_0(x,y) = \sum_{n=-\infty,n\neq 0}^{n=+\infty} \hat{\hat{\theta}}_0^{(n)}(y)\mathrm{e}^{\mathrm{i}n\alpha x}$$
$$= \sum_{n=-\infty,n\neq 0}^{n=+\infty} \frac{\theta_L^{(n)}}{\cosh(2n\alpha)} [\cosh(n\alpha y)\cosh(n\alpha) - \sinh(n\alpha y)\sinh(n\alpha)]\,\mathrm{e}^{\mathrm{i}n\alpha x}. \quad (\mathrm{D}\,1)$$

The field equations take the form

$$(Reu_0+u_1)\frac{\partial u_1}{\partial x} + Rev_1\frac{\mathrm{d}u_0}{\mathrm{d}y} + v_1\frac{\partial u_1}{\partial y} = -\frac{\partial p_1}{\partial x} + \frac{\partial^2 u_1}{\partial x^2} + \frac{\partial^2 u_1}{\partial y^2}, \quad (\mathrm{D}\,2a)$$

$$(Reu_0+u_1)\frac{\partial v_1}{\partial x} + v_1\frac{\partial v_1}{\partial y} = -\frac{\partial p_1}{\partial y} + \frac{\partial^2 v_1}{\partial x^2} + \frac{\partial^2 v_1}{\partial y^2} + Ra_{per}\theta_1 + Ra_{per}Pr^{-1}\hat{\hat{\theta}}_0, \quad (\mathrm{D}\,2b)$$

$$(Reu_0+u_1)\left(\frac{\partial \hat{\hat{\theta}}_0}{\partial x} + Pr\frac{\partial \theta_1}{\partial x}\right) + v_1\left(\frac{\partial \hat{\hat{\theta}}_0}{\partial y} + Pr\frac{\partial \theta_1}{\partial y}\right) = \frac{\partial^2\theta_1}{\partial x^2} + \frac{\partial^2\theta_1}{\partial y^2}, \quad (\mathrm{D}\,2c)$$

$$\frac{\partial u_1}{\partial x} + \frac{\partial v_1}{\partial y} = 0 \quad (\mathrm{D}\,2d)$$

and are supplemented by the boundary conditions

$$u_1(\pm 1) = 0, \quad v_1(\pm 1) = 0, \quad \theta_1(-1) = 0, \quad \partial\theta_1/\partial y(1) = 0 \quad (\mathrm{D}\,3a\text{–}d)$$

and the constraint (2.7). The above system is solved using the method described in § 3.

REFERENCES

Bergman, T. L., Lavine, A. S., Incropera, F. P. & Dewitt, D. P. 2011 *Fundamentals of Heat and Mass Transfer*, 7th edn. Wiley.

Bewley, T. 2009 A fundamental limit on the balance of power in a transpiration-controlled channel flow. *J. Fluid Mech.* **632**, 443–446.

Chandrasekhar, S. 1961 *Hydrodynamic and Hydromagnetic Stability*. Oxford University Press.

Choi, H., Moin, P. & Kim, J. 1991 On the effect of riblets in fully developed laminar channel flows. *Phys. Fluids* A **3**, 1892–1896.

Chu, D. C. & Karniadakis, G. 1993 A direct numerical simulation of laminar and turbulent flow over riblet-mounted surfaces. *J. Fluid Mech.* **250**, 1–42.

Fiebig, M. 1995 Embedded vortices in internal flow: heat transfer and pressure loss enhancement. *Intl J. Heat Fluid Flow* **16**, 376–388.

Floryan, J. M. 2012 The thermo-superhydrophobic effect. *Bull. Am. Phys. Soc.* **57** (1), X50.00015.

Freund, G., Pesch, W. & Zimmermann, W. 2011 Rayleigh–Bénard convection in the presence of spatial temperature modulations. *J. Fluid Mech.* **673**, 318–348.

Fukugata, K., Sugiyama, K. & Kasagi, N. 2009 On the lower bound of net driving power in controlled duct flows. *Physica* D **238**, 1082–1086.

Gage, K. S. & Reid, W. H. 1968 The stability of thermally stratified plane Poiseuille flow. *J. Fluid Mech.* **33**, 21–32.

HOSSAIN, M. Z., FLORYAN, D. & FLORYAN, J. M. 2012 Drag reduction due to spatial thermal modulations. *J. Fluid Mech.* **713**, 398–419.

HOSSAIN, M. Z. & FLORYAN, J. M. 2013 Instabilities of natural convection in a periodically heated layer. *J. Fluid Mech.* **733**, 33–67.

JACOBI, A. M. & SHAH, R. K. 1998 Air-side flow and heat transfer in compact heat exchangers: a discussion of enhancement mechanisms. *Heat Transfer Engng* **19**, 29–41.

JOSEPH, P., COTTIN-BIZONNE, C., BENOIT, J. M., YBERT, C., JOURNET, C., TABELING, P. & BOCQUET, L. 2006 Slippage of water past superhydrophobic carbon nanotube forests in microchannels. *Phys. Rev. Lett.* **97**, 156104.

KIERZENKA, J. & SHAMPINE, L. F. 2001 A BVP solver based on residual control and the MATLAB PSE. *ACM Trans. Math. Softw.* **27**, 299–316.

KIERZENKA, J. & SHAMPINE, L. F. 2008 A BVP solver that controls residual and error. *J. Numer. Anal. Ind. Appl. Maths* **3**, 27–41.

LIGRANI, P. M., OLIVIERA, M. M. & BLASKOVICH, T. 2003 Comparison of heat transfer augmentation techniques. *AIAA J.* **41**, 337–362.

MOHAMMADI, A. & FLORYAN, J. M. 2012 Mechanism of drag generation by surface corrugation. *Phys. Fluids* **24**, 013602.

MOHAMMADI, A. & FLORYAN, J. M. 2013*a* Pressure losses in grooved channels. *J. Fluid Mech.* **725**, 23–54.

MOHAMMADI, A. & FLORYAN, J. M. 2013*b* Groove optimization for drag reduction. *Phys. Fluids* **25**, 113601.

ORSZAG, S. A. 1971 Accurate solutions of the Orr–Sommerfeld stability equation. *J. Fluid Mech.* **50**, 689–704.

OU, J., PEROT, J. B. & ROTHSTEIN, J. P. 2004 Laminar drag reduction in microchannels using ultrahydrophobic surfaces. *Phys. Fluids* **16**, 4635–4643.

OU, J. & ROTHSTEIN, J. P. 2005 Direct velocity measurements of the flow past drag-reducing ultrahydrophobic surfaces. *Phys. Fluids* **17**, 103606.

QUÉRÉ, D. 2008 Wetting and roughness. *Annu. Rev. Mater. Res.* **38**, 71–99.

REYSSAT, M., YEOMANS, J. M. & QUÉRÉ, D. 2008 Impalement of fakir drops. *Europhys. Lett.* **81**, 26006.

ROTHSTEIN, J. P. 2010 Slip on superhydrophobic surfaces. *Annu. Rev. Fluid Mech.* **42**, 89–109.

SAMAHA, M. A., TAFRESHI, H. V. & GAD-EL-HAK, M. 2011 Modeling drag reduction and meniscus stability of superhydrophobic surfaces comprised of random roughness. *Phys. Fluids* **23**, 012001.

TAKAGI, D. & BALMFORTH, N. J. 2011 Peristaltic pumping of viscous fluid in an elastic tube. *J. Fluid Mech.* **672**, 196–218.

TRUESDELL, R., MAMMOLI, P., VOROBIEFF, P., VAN SWOL, P. & BRINKER, C. J. 2006 Drag reduction on a patterned superhydrophobic surface. *Phys. Rev. Lett.* **97**, 044504.

YAMAMOTO, A., HASEGAWA, Y. & KASAGI, N. 2013 Optimal control of dissimilar heat and momentum transfer in fully developed turbulent channel flow. *J. Fluid Mech.* **733**, 189–230.

ZHOU, M., LI, J., WU, C., ZHOU, X. & CAI, L. 2011 Fluid drag reduction on superhydrophobic surfaces coated with carbon nanotube forest (CNTs). *Soft Matt.* **7**, 4391–4396.